Received: 31 July 2023 | Revised: 11 March 2024 | Accepted: 11 March 2024

DOI: 10.1111/mmi.15253

RESEARCH ARTICLE

WILEY

An essential protease, FtsH, influences daptomycin resistance acquisition in *Enterococcus faecalis*

Zeus Jaren Nair[1,2,3,4] | Iris Hanxing Gao[2,4] | Aslam Firras[2,4] | Kelvin Kian Long Chong[2,3] | Eric D. Hill[5] | Pei Yi Choo[2,4] | Cristina Colomer-Winter[6] | Qingyan Chen[2,4] | Caroline Manzano[6] | Kevin Pethe[1,2,7,8] | Kimberly A. Kline[1,2,4,6]

[1]Singapore-MIT Alliance for Research and Technology, Antimicrobial Drug Resistance Interdisciplinary Research Group, Singapore, Singapore

[2]Singapore Centre for Environmental Life Sciences Engineering, Nanyang Technological University, Singapore, Singapore

[3]Interdisciplinary Graduate Programme, Graduate College, Nanyang Technological University, Singapore, Singapore

[4]School of Biological Sciences, Nanyang Technological University, Singapore, Singapore

[5]Singapore Centre for Environmental Life Sciences Engineering, National University of Singapore, Singapore, Singapore

[6]Department of Microbiology and Molecular Medicine, University of Geneva, Geneva, Switzerland

[7]Lee Kong Chian School of Medicine, Nanyang Technological University, Singapore, Singapore

[8]National Centre for Infectious Diseases (NCID), Singapore, Singapore

Correspondence
Kimberly A. Kline, Department of Microbiology and Molecular Medicine, University of Geneva, Geneva, Switzerland.
Email: kimberly.kline@unige.ch

Funding information
Ministry of Education - Singapore, Grant/Award Number: MOE2017-T1-001-269; Singapore-MIT Alliance for Research and Technology (SMART) Centre; National Medical Research Council, Grant/Award Number: MOH-000645; Schweizerischer Nationalfonds zur Förderung der Wissenschaftlichen Forschung, Grant/Award Number: 310030_212262; Singapore Centre for Environmental Life Sciences Engineering (SCELSE)

Abstract

Daptomycin is a last-line antibiotic commonly used to treat vancomycin-resistant Enterococci, but resistance evolves rapidly and further restricts already limited treatment options. While genetic determinants associated with clinical daptomycin resistance (DAP^R) have been described, information on factors affecting the speed of DAP^R acquisition is limited. The multiple peptide resistance factor (MprF), a phosphatidylglycerol-modifying enzyme involved in cationic antimicrobial resistance, is linked to DAP^R in pathogens such as methicillin-resistant *Staphylococcus aureus*. Since *Enterococcus faecalis* encodes two paralogs of *mprF* and clinical DAP^R mutations do not map to *mprF*, we hypothesized that functional redundancy between the paralogs prevents *mprF*-mediated resistance and masks other evolutionary pathways to DAP^R. Here, we performed in vitro evolution to DAP^R in *mprF* mutant background. We discovered that the absence of *mprF* results in slowed DAP^R evolution and is associated with inactivating mutations in *ftsH*, resulting in the depletion of the chaperone repressor HrcA. We also report that *ftsH* is essential in the parental, but not in the Δ*mprF*, strain where FtsH depletion results in growth impairment in the parental strain, a phenotype associated with reduced extracellular acidification and reduced ability for metabolic reduction. This presents FtsH and HrcA as enticing targets for developing anti-resistance strategies.

KEYWORDS
chaperones, Daptomycin resistance, *Enterococcus faecalis*, *ftsH*, *hrcA*, multiple peptide resistance factor (*mprF*)

1 | INTRODUCTION

Enterococci are a major healthcare concern due to their association with hospital acquired infections (HAIs). Enterococci accounted for 14% of all HAIs in the United States from 2011 to 2014 and 10% of HAIs in Europe in 2010, where *Enterococcus faecalis* comprise the majority of enterococcal HAIs, contributing up to 64.7% globally from 1997 to 2016 (Pfaller et al., 2019; Weiner et al., 2016; Zarb et al., 2012). Enterococci cause a variety of infections including catheter-associated infections (CAUTI), endocarditis, peritonitis, colitis, diabetic foot ulcers, surgical site infections (Edmond et al., 1999; Hidron et al., 2008; Murdoch et al., 2009; Patterson et al., 1995; Weiner et al., 2016). Many of these infections are biofilm-associated, rendering them inherently more tolerant to antibiotics and difficult to treat (Ch'ng et al., 2019).

An additional challenge in treating Enterococcal infections is their intrinsic and acquired resistance to antimicrobials, including last-line drugs such as vancomycin (Hollenbeck & Rice, 2012; Miller et al., 2014). For example, infections caused by vancomycin-resistant Enterococci (VRE) are associated with increased mortality rates, lengthened hospital stays, and higher treatment and infection control costs (Carmeli et al., 2002; Mascini & Bonten, 2005; Miller et al., 2020; Prematunge et al., 2016; Reinseth et al., 2020; Song et al., 2003). Treatment of VRE infections typically involves the use of antibiotics of last resort such as linezolid and daptomycin (Patel & Gallagher, 2015). Daptomycin (DAP) is a lipopeptide antibiotic with broad activity against Gram-positive bacteria. It is positively charged when complexed with its calcium cofactor and targets the negatively charged bacterial membrane wherein it oligomerizes to cause membrane disruption, ion leakage, and eventual cell death (Steenbergen et al., 2005; Taylor & Palmer, 2016). Daptomycin bactericidal activity is also conferred by its ability to disrupt fluid membrane microdomains during membrane insertion. This results in delocalization of proteins essential for cell wall synthesis that are located within these fluid domains. Daptomycin membrane insertion also causes clustering of fluid lipids resulting in hydrophobic mismatch between fluid and rigid membrane domains that cause proton leakage and membrane depolarization (Müller et al., 2016). Although DAP is typically effective in treating VRE infections, VRE can also acquire daptomycin resistance (DAP^R), further reducing the already limited treatment options (Arias & Murray, 2012; Kelesidis et al., 2011; Miller et al., 2020; Munita et al., 2014; Munoz-Price et al., 2005; Shoemaker et al., 2006). While the rate of resistance to DAP in Enterococci is still relatively low at 0.1% for *E. faecalis* and 9% for *E. faecium*, DAP^R co-occurrence with VRE has been reported in several meta-analyses in Australia and New Zealand from 2007 to 2018, where 15% of vancomycin-resistant *E. faecium* are DAP^R, and globally from 2003 to 2010, 93.3% of Enterococcal DAP^R were VRE (Dadashi et al., 2021; Kelesidis et al., 2011; Li et al., 2021).

Given the clinical importance of DAP as a therapeutic and the emerging threat of resistance, enterococcal DAP^R-associated mutations and resistance mechanisms have been characterized. Diverse genetic changes have been associated with DAP^R in both clinical isolates and in vitro settings. In vancomycin-resistant *E. faecalis* DAP^R patient isolates, mutations were identified in *liaF* (the negative regulator of the LiaFSR three-component system), *gdpD* (glycerophosphodiesterase), and *cls* (cardiolipin synthase), and similar mutations in all three genes were recapitulated in in vitro evolution of DAP-sensitive isolates to DAP^R (Arias et al., 2011; Miller et al., 2013; Palmer et al., 2011). Additionally, in vitro evolution also revealed DAP^R-associated mutations not observed in clinical isolates such as in genes related to oxidative stress response (*gsh*, *yybT*, *selA*) and drug efflux (*mdpA*) (Miller et al., 2013). Similarly, mutations in *cls* and *liaFSR* have also been associated with DAP^R in *E. faecium* from both in vivo clinical isolates and in vitro evolution of DAP-sensitive strains to DAP^R (Li et al., 2022; Sinel et al., 2016; Tran, Panesso, Gao, et al., 2013; Wang et al., 2018). Mutations in *liaF* as well as in *yvlB* (a putative LiaFSR target) in DAP^R strains suggest involvement of LiaFSR-mediated membrane stress sensing (Arias et al., 2011, Miller et al., 2013). DAP^R-associated mutations in *gdpD* and *cls*, decreased levels of phosphatidylglycerol (PG) and increased glycerophosphoryl-diglucosyldiacylglycerol (GPDGDAG), together with increased membrane rigidity and diversion of daptomycin away from the septum in DAP^R strains suggest that DAP^R is mediated through membrane remodeling (Arias et al., 2011; Mishra et al., 2012; Rashid et al., 2017; Tran, Panesso, Mishra, et al., 2013). Further investigation showed that LiaFSR is indeed one of the key systems that senses antimicrobials and initiates membrane remodeling to confer antibiotic resistance in *E. faecalis* (Khan et al., 2019). Taken together, these mutations suggest common DAP^R mechanisms among Enterococci involving antimicrobial stress sensing and membrane remodeling.

Despite the current advances in understanding DAP^R resistance mechanisms, information on factors that influence the rate of DAP^R acquisition is scarce. A complete understanding of DAP^R in terms of both factors directly affecting resistance and factors that influence the speed and likelihood of progression toward resistance are equally important in the pursuit of anti-resistance strategies to mitigate potential widespread resistance in the future.

DAP^R has been similarly well-studied in *Staphylococcus aureus*, where DAP^R is associated with *mprF* gain-of-function mutations and increased expression (Ernst et al., 2018; Mishra et al., 2009; Sabat et al., 2018; Sulaiman & Lam, 2021). Multiple peptide resistance factor (MprF) is a membrane-bound enzyme that aminoacylates phosphatidylglycerol (PG) in the inner leaflet of the membrane and flips

it to the outer leaflet, resulting in a reduction in the overall negative charge of the membrane and giving rise to electrostatic repulsion of cationic antimicrobials (Bao et al., 2012; Ernst & Peschel, 2011; Rashid et al., 2016). Multiple peptide resistance factor mutations have not been reported in association with enterococcal DAP^R. While there is only one *mprF* gene in the *S. aureus* genome, *E. faecalis* and *E. faecium* encode two paralogs—MprF1 and MprF2—where MprF2 appears to be the major contributor to PG aminoacylation in *E. faecalis* (Bao et al., 2012; Rashid et al., 2023). We have also reported that *mprF* is closely tied to global lipidome regulation and cell physiology, and the absence of *mprF* significantly alters membrane lipid composition resulting in altered membrane fluidity, reduced secretion, and increased dependence on exogenous fatty acids (Rashid et al., 2023). Given its daptomycin protective effects, we hypothesized that MprF redundancy afforded by its two encoding orthologues may mask additional daptomycin resistance events that occur during in vitro and in vivo evolution of *E. faecalis* to DAP^R.

To investigate this possibility, we conducted in vitro evolution to DAP^R in *mprF* mutant backgrounds and discovered DAP^R-associated mutations in several genes not previously associated with DAP^R, including *ftsH*. FtsH is a conserved protease, and DAP^R-associated mutations were only enriched in a Δ*mprF1* Δ*mprF2* background. Our data show that *ftsH* is essential in parental *E. faecalis* but not in the Δ*mprF1* Δ*mprF2* strain where its inactivation contributes to slowed evolution to DAP^R. We found that FtsH indirectly affects the levels of the repressor of chaperone operons (HrcA), which in turn influences the speed of DAP^R evolution. These findings provide evidence for a role of FtsH activity and HrcA in influencing DAP^R acquisition.

TABLE 1 Daptomycin minimal inhibitory concentrations (MICs).

Strain	MIC in BHI (μg/mL)
Wild-type *E. faecalis* (OG1RF)	4–8
Δ*mprF1*	4–8
Δ*mprF2*	2–4
Δ*mprF1* Δ*mprF2*	2
Δ*mprF1* Δ*mprF2* passage control	16
Δ*mprF1* Δ*mprF2 ftsH*(G37X)	8
trePP::Tn	4
gelE::Tn	4
yckE::Tn	4
cryZ::Tn	4
hrcA::Tn	2
lutA::Tn	4
carB::Tn	4
dnaJ::Tn	4
groEL::Tn	8
Δ*dnaK*	4
Δ*liaR*	0.5–1
Δ*liaFSR*	0.5
cls1::Tn Δ*cls2*	4
Strain	**MIC in MHB II (μg/mL)**
Wild-type *E. faecalis* (OG1RF)	2
Δ*mprF1*	1–2
Δ*mprF2*	1
Δ*mprF1* Δ*mprF2*	1

2 | RESULTS

2.1 | Mutations in *ftsH* are enriched in Δ*mprF1* Δ*mprF2* during in vitro evolution to DAP^R

Since MprF activity contributes to DAP^R in *S. aureus*, we investigated the contribution of the *E. faecalis mprF* paralogs to DAP^R (Ernst et al., 2018; Mishra et al., 2009; Sabat et al., 2018). Based on DAP breakpoints for *E. faecalis* of ≤2 μg/mL (susceptible), 4 μg/mL (intermediate), and ≥8 μg/mL (resistant) as listed by the Clinical and Laboratory Standards Institute (CLSI) (Satlin et al., 2019), the *E. faecalis* OG1RF strain used in this study is in the susceptible range for DAP resistance given its MIC of 2 μg/mL (Table 1). While the strain of *E. faecalis* used in this study is susceptible to DAP, a further deletion of *mprF* makes this strain hypersensitive to DAP relative to the wild-type parental strain, reducing the MIC in MHB II by twofold in Δ*mprF2* and Δ*mprF1* Δ*mprF2*, and in BHI by two-to fourfold in Δ*mprF2* and fourfold in Δ*mprF1* Δ*mprF2* (Table 1). Hence, we hypothesized that the DAP-protective activity of MprF may mask resistance-associated mutations not previously detected in DAP^R clinical isolates and in vitro evolution studies.

To test this hypothesis, we performed in vitro evolution to DAP^R in *mprF* single and double mutants. Strains were first grown with DAP concentrations at 0.5X, 1X, and 2X their respective MIC. The highest DAP concentration in which cultures grew was defined as the highest growth permissive concentration (HGPC) for the first round. In the following round, cultures were grown at 0.5X, 1X, and 2X of the preceding day's HGPC. This was done successively until an end point HGPC of 512 μg/mL DAP was achieved (Figure 1a). Using this approach, we were able to track the progression to DAP^R over time by recording the HGPC values. We observed that wild-type and Δ*mprF1* reached the end point HGPC at similar rates and times, whereas Δ*mprF2* and Δ*mprF1* Δ*mprF2* progressed more slowly (Figure 1b). While Δ*mprF2* and Δ*mprF1* Δ*mprF2* reached end point resistance at similar times, Δ*mprF1* Δ*mprF2* displayed slower evolution in the initial phases from Day 1 to Day 15 as compared to Δ*mprF2*. This, however, cannot be fully explained by differences in phenotypic mutation rate since the mutation rates of the *mprF* mutants are not significantly different from the wild-type (Figure 1c).

Clonal isolates were collected daily throughout evolution and sequenced to identify resistance-associated mutations in each genetic background (Figure 1d; File S1a,b). Mutations in cardiolipin synthase genes (*cls1*, *cls2*), previously implicated in *E. faecalis* DAP^R (Arias et al., 2011; Miller et al., 2013), emerged during the intermediate stages of evolution (DAP HGPC of 16–64 μg/mL) in all genetic backgrounds. We did not observe enrichment of mutations in genes

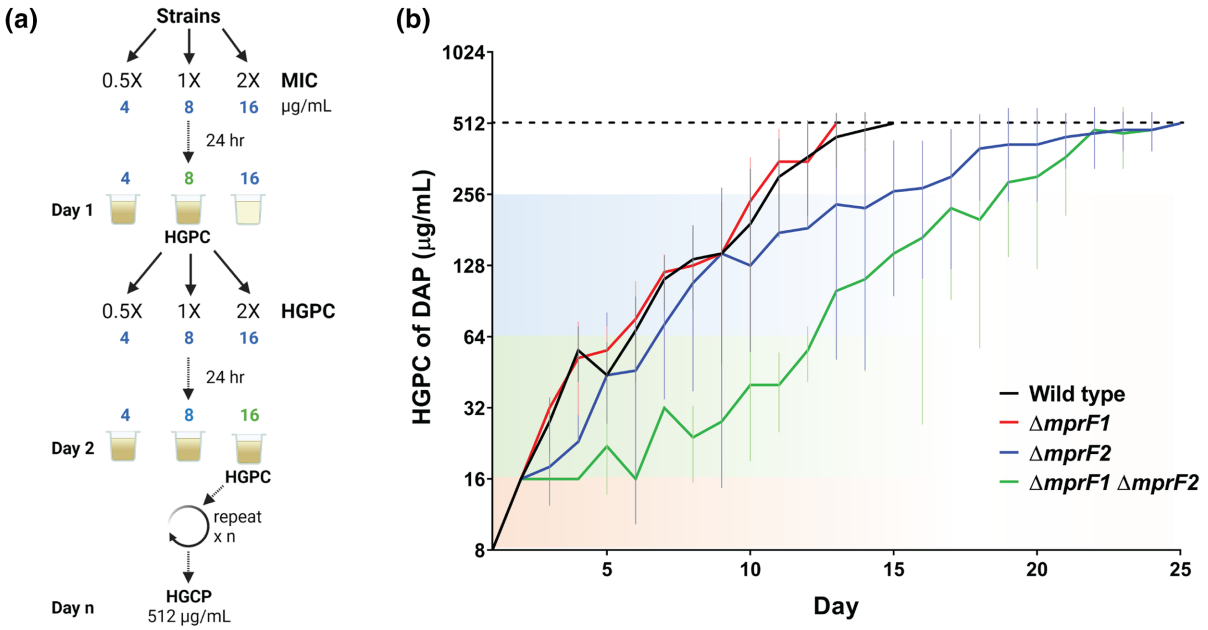

(c)

Mutation rate of *mprF* mutants		
Mutant	**Mean mutation rate**	**Adjusted p-values**
Wild type	$3.80 \times 10^{-8} \pm 2.43 \times 10^{-8}$	-
Δ*mprF1*	$4.16 \times 10^{-8} \pm 2.98 \times 10^{-8}$	0.870
Δ*mprF2*	$1.21 \times 10^{-8} \pm 8.39 \times 10^{-9}$	0.216
Δ*mprF1* Δ*mprF2*	$6.10 \times 10^{-9} \pm 5.24 \times 10^{-9}$	0.104

(d)

Genes where mutations commonly occur				
Gene ID (new)	**Gene ID (old)**	**Identity**	**Sequence of occurrence**	**Enriched in which strain?**
RS01045	OG1RF_10209	*ftsH*	Early	Δ*mprF1* Δ*mprF2*
RS01975 RS06840	OG1RF_10364 OG1RF_11324	*cls1, cls2*	Intermediate	All
RS07535	OG1RF_11464	*liaX*	Intermediate	Wild type Δ*mprF1* Δ*mprF2*
RS07740	OG1RF_11507	Putative membrane protein	Intermediate	Wild type Δ*mprF1*
RS02330	OG1RF_10437	Putative AI-2E family transporter	Late	Δ*mprF1* Δ*mprF2*
RS09725	OG1RF_11901	Putative HD domain protein	Late	Wild type Δ*mprF1*

Early, ≤16 µg/mL; Intermediate, ≤64 µg/mL; Late, ≤256 µg/mL

FIGURE 1 In vitro evolution of *mprF* mutants to DAP^R reveal novel mutations. (a) Workflow for in vitro evolution. Strains to be evolved were first grown in media supplemented with 0.5X, 1X or 2X their respective DAP MIC (e.g., 4, 8, 16 µg/mL) for 24 hours. The highest concentration of DAP that allowed for growth is termed the highest growth permissive concentration (HGPC) (e.g., 8 µg/mL). In the following passage, the HGPC culture was subcultured at 0.5X, 1X, 2X the HGPC of DAP (e.g., 4, 8, 16 µg/mL). This is repeated continually until an endpoint HGCP of 512 µg/mL of DAP was achieved. (b) The mean HGPC of daptomycin over time for each strain is plotted against time. Error bars indicate standard deviation from eight parallel lines of evolution. (c) Mean mutation rate with standard deviation of *mprF* mutants from three replicates from independent experiments assayed by the Luria-Delbrück fluctuation assay which measures phenotypic mutation rates. Comparisons were made for each mutant against the wild type. Significance tested by permutation (10,000 shuffles within experimental groups to preserve the integrity of the experimental design) with Benjamini–Hochberg adjusted *p*-values to control false discovery in multiple comparisons. (d) Whole-genome sequencing across evolution reveals an ordered progression of acquired mutations, with enrichment of some mutants in specific mutant backgrounds. The sequence of occurrence of mutations is based of DAP HGPC where the mutation first occurred (early, ≤16 µg/mL; intermediate, ≤64 µg/mL; Late, ≤256 µg/mL). Detailed information of all mutations observed are displayed relative to sequence of occurrence in evolution in File S1a, and relative to number of observed occurrences per gene in File S1b.

encoding the LiaFSR three-component system as described previously in DAP^R strains (Arias et al., 2011, Miller et al., 2013); however, mutations in the gene encoding LiaX—an antimicrobial sensing component for LiaFSR (Arias et al., 2011; Khan et al., 2019; Miller et al., 2013; Reyes et al., 2015) arose at a similar intermediate time in all genetic backgrounds except Δ*mprF1* Δ*mprF2* (Figure 1d).

Mutations in *liaX* have previously been detected in an in vitro evolution screen where the gene was annotated as "EF1753, conserved hypothetical protein," and more recently detected in DAP^R *E. faecalis* clinical isolates (Ota et al., 2021; Palmer et al., 2011). Mutations in genes encoding a predicted membrane protein (RS07740) and predicted HD domain protein (RS09725) were observed at intermediate and later stages of evolution (DAP HGPC >64 μg/mL), respectively, and in the wild-type and Δ*mprF1* background. Additionally, mutation in a predicted AI-2E family transporter (RS02330) was also observed at later stages of evolution (DAP HGPC ≤256 μg/mL) only in the Δ*mprF1* Δ*mprF2* background. Interestingly, mutations in *ftsH* were only observed in the Δ*mprF1* Δ*mprF2* background, during the earliest stages of evolution (DAP HGPC ≤16 μg/mL) (Figure 1d). FtsH is a conserved ATP-dependent zinc-metalloprotease and is membrane bound and hexameric in nature (Bieniossek et al., 2006; Langklotz et al., 2012). The cellular processes that FtsH influences are diverse across different organisms and depends largely on the substrates that it targets (Deuerling et al., 1997; Kamal et al., 2019; Okuno & Ogura, 2013; Yepes et al., 2012). FtsH was chosen for further investigation due to the intriguing phenomenon where mutations are enriched in the Δ*mprF1* Δ*mprF2* background. The mutations in the other genes were not investigated in detail as their functions in DAP^R are either already known in the case of *cls*, and *liaX* or protein identity and detailed functions are not well defined in the case of the remaining genes RS07740, RS02330, and RS09725.

2.2 | FtsH is essential in the wild-type but not Δ*mprF1* Δ*mprF2*

Many of the DAP^R-associated *ftsH* mutations encode point mutations clustered within the ATP-binding site of the AAA+ domain or result in a G37X nonsense mutation near the N-terminal region of *ftsH*, suggesting that these mutations likely result in a loss of function (Figure 2a).To determine the contribution of *ftsH* mutations in DAP^R evolution, the *ftsH*(G37X) loss-of-function truncate was chosen for introduction into the wild-type and Δ*mprF1* Δ*mprF2* backgrounds on a plasmid using a constitutive sortase A promoter

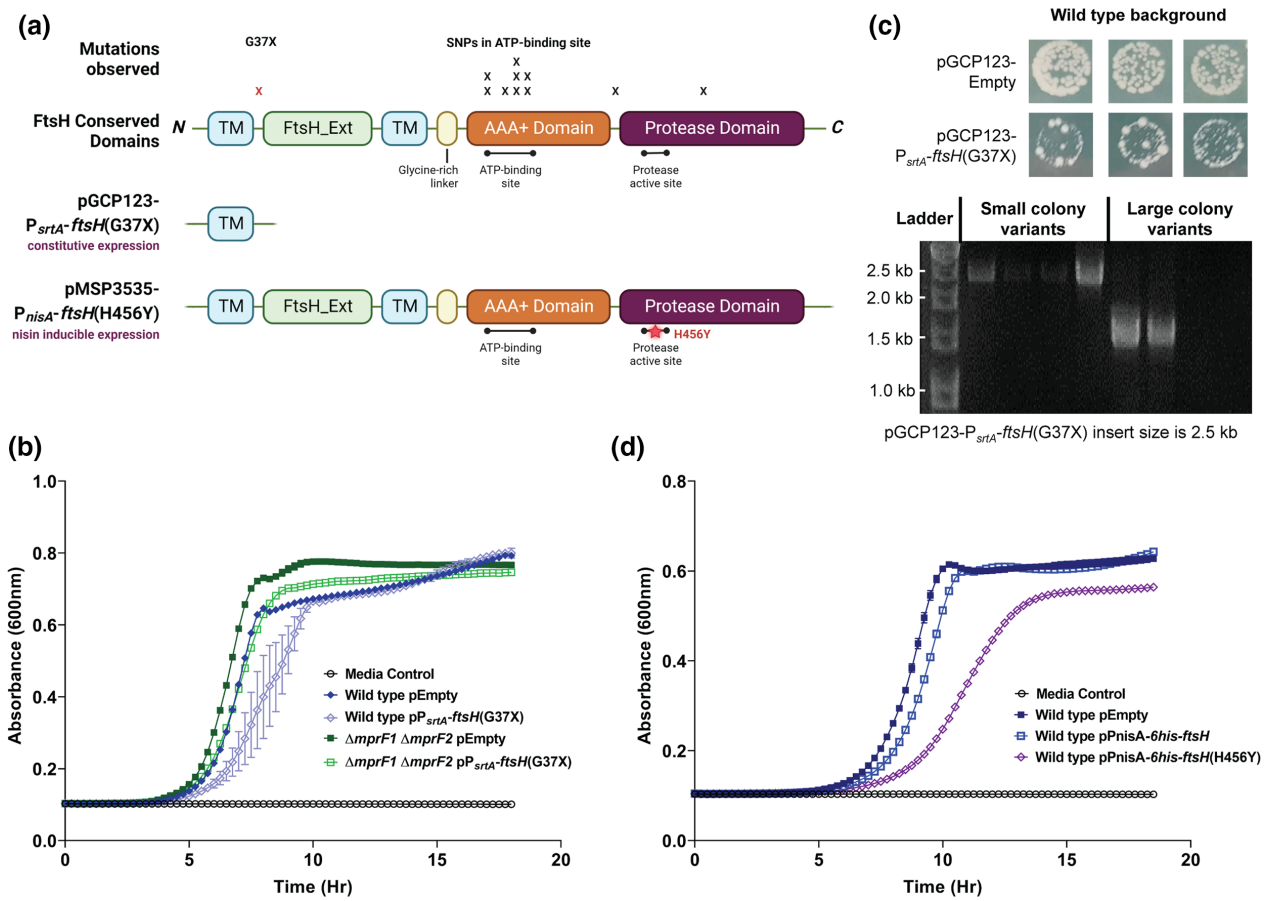

FIGURE 2 Mutations in *ftsH* are conditionally permissible in Δ*mprF1* Δ*mprF2*. (a) Map of single nucleotide polymorphism (SNP) mutations frequently observed in *ftsH* through evolution overlaid on where they occur with reference to conserved domains of FtsH. Diagrams showing the *ftsH* variants expressed—truncated FtsH(G37X) under constitutive expression (P_{srtA}) or full length but proteolytically inactive FtsH(H456Y) under nisin inducible expression (P_{nisA}). Created with BioRender.com. (b) Growth curves of wild-type and Δ*mprF1* Δ*mprF2* with *ftsH*(G37X) expression. (c) *ftsH*(G37X) expression results in small and large colony variants in the wild-type, where large colony variants show reduced/absent inserts within the expression vector. (d) Growth curves of the wild-type with induced expression of either active *ftsH* or proteolytically inactive *ftsH*(H456Y). Error bars represent the standard error of mean from three biological replicates.

(pGCP123-P_{srtA}) (Figure 2a). Since FtsH forms homohexamers, we expected that *FtsH*(G37X) would assemble with native, chromosomally encoded FtsH, causing dominant negative dysfunction of the enzyme complex (Langklotz et al., 2012; Liu et al., 2022; Niwa et al., 2002). Indeed, the expression of *ftsH*(G37X) resulted in slowed growth in wild-type, but not Δ*mprF1* Δ*mprF2* mutant cells (Figure 2b). Within the wild-type *ftsH*(G37X) expressing strain, log phase absorbance values were more variable than for the control strains (Figure 2b). We also noticed that small and large colony variants were only present in the wild-type *ftsH*(G37X) expressing strain and subsequent analysis revealed loss of or reduced *ftsH*(G37X) insert sizes within the large colony variants but not the small colony variants (Figure 2c). These results suggest that FtsH loss-of-function (FtsH-LoF) is not tolerated in the wild-type strain, but is permissible in Δ*mprF1* Δ*mprF2*. To confirm this, a proteolytically inactive *ftsH* variant—*ftsH*(H456Y) in which the conserved zincin motif within the protease active site was mutated as described by others—was constructed and placed under nisin inducible expression in a plasmid (pMSP3535-P_{nisA}) (Arends et al., 2016; Bieniossek et al., 2006) (Figure 2a). As predicted, induction of 6his-*ftsH*(H456Y) in the wild-type background resulted in slowed growth while the expression of 6his-*ftsH* showed similar growth as the empty vector control (Figure 2d). Moreover, attempts to introduce the *ftsH*(G37X) mutation into the chromosome were unsuccessful in the wild-type background, but was possible in Δ*mprF1* Δ*mprF2* (data not shown). Taken together, these data show that *ftsH* is essential in a wild-type background and its LoF is tolerated only in a Δ*mprF1* Δ*mprF2* genetic background.

2.3 | FtsH-LoF leads to metabolic impairments

To understand why an FtsH-LoF mutation caused a growth defect only in the wild-type genetic background, we examined the viability of cells constitutively expressing *ftsH*(G37X) or inducibly expressing *ftsH*(H456Y). We observed similar proportions of propidium iodide (PI) stained cells in both populations, suggesting that membrane permeability is not affected by FtsH-LoF (Figure S1a). We also observed an increase in cell chaining upon FtsH-LoF in the wild-type (Figure S1b).

To gain further insight into FtsH-dependent growth defects, we performed RNA sequencing following induced expression of either 6his-*ftsH* or 6his-*ftsH*(H456Y). However, we did not observe any obvious expression differences in genes that would explain this phenomenon (File S1c). Despite the lack of insight from the transcriptomics data, we reasoned that the viability is unlikely to be affected since we observed no differences in PI staining and considered whether the slowed growth could be driven by altered metabolism. We therefore assessed the ability of the FtsH-LoF strains to reduce the resazurin dye to a fluorescent product using the Alamar blue assay as an indicator of electron flow in the membrane. We observed a decrease in fluorescence of the reduced resazurin dye in the wild-type strain constitutively expressing *ftsH*(G37X) as well as with induced expression of *ftsH*(H456Y), suggesting impairment in reductive metabolic activity when FtsH LoF occurs (Figure 3a,b).

We next considered the possibility that a shift in dominant cell metabolic pathways might explain the reduced metabolic activity. We performed Agilent Seahorse real-time cell metabolic analysis of extracellular acidification rates (ECAR) as an indirect measure of glycolysis, and oxygen consumption rate (OCR) as an indirect measure of oxidative phosphorylation in mid log phase cultures of wild-type and Δ*mprF1* Δ*mprF2* expressing both constitutive and induced expression of inactive *ftsH* variants. FtsH-LoF correlated with significantly reduced ECAR indicating reduced media acidification following the expression of inactive *ftsH* variants (Figure 3c–e). This was observed for both constitutive and inducible expression of FtsH inactive variants, and in both the wild-type and Δ*mprF1* Δ*mprF2*. Hence, these data indicate a generalized decrease in ability to acidify the media under FtsH-LoF (Figure 3c–e). The Seahorse OCR measurements were also largely similar across all strains indicating similar oxidative phosphorylation rates (Figure S2a). FtsH-LoF also did not result in any significant changes in quantified ATP levels (Figure S2b). Overall, these findings suggest that reduced growth of wild-type cells expressing FtsH-LoF could be caused by reduced ability for metabolic reduction. Although the mechanism behind this phenomenon is unclear, we can rule out the contribution of oxidative phosphorylation and ATP production since they are similar across all strains.

2.4 | Speed of evolution to DAP^R is slowed under FtsH-LoF

Given that *ftsH* mutations were observed early in the slowed evolution of Δ*mprF1* Δ*mprF2* toward DAP^R, we reasoned that these FtsH-LoF mutations might either be the reason for the slowed evolution or could be priming Δ*mprF1* Δ*mprF2* to acquire other DAP^R-associated mutations in the later stages (Figure 1). Thus, the *ftsH*(G37X) mutation was introduced into the genome of Δ*mprF1* Δ*mprF2* for further investigation. As several days of passaging were carried out in low concentrations of DAP to encourage homologous recombination and retention of the *ftsH*(G37X) mutation in Δ*mprF1* Δ*mprF2*, a parallel culture of Δ*mprF1* Δ*mprF2* was passaged under the same conditions to serve as a control strain for comparisons in subsequent assays. This strain will be referred to henceforth as Δ*mprF1* Δ*mprF2* passage control. Δ*mprF1* Δ*mprF2 ftsH*(G37X) and Δ*mprF1* Δ*mprF2* passage control were subjected to in vitro evolution to DAP^R where we observed that Δ*mprF1* Δ*mprF2 ftsH*(G37X) evolved at a slower speed than Δ*mprF1* Δ*mprF2*, where under FtsH-LoF, the HGPC values were lower than the passage control at almost all time points and an additional 5 days was required to reach end point HGPC (Figure 4a). Since Δ*mprF1* Δ*mprF2 ftsH*(G37X) displayed a twofold lower DAP MIC as compared to the Δ*mprF1* Δ*mprF2* passage control, it was possible that the increased DAP sensitivity at the outset of the experiment could explain the slowed evolution (Table 1). Thus, we calculated the fold-change of HGPC over time relative to the initial HGPC value at Day 1 (Figure 4b). The HGPC fold-change progression over time

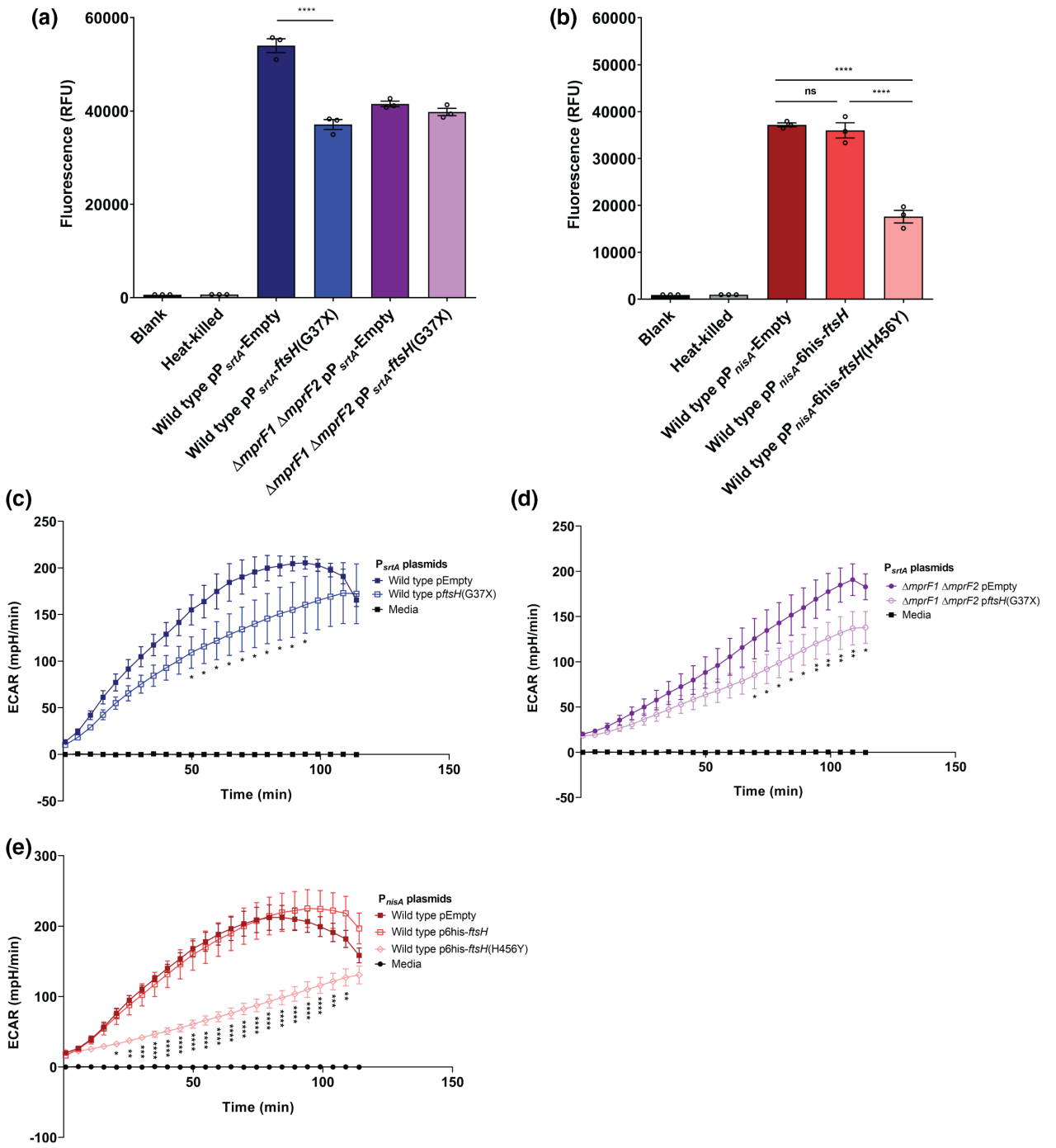

FIGURE 3 FtsH loss of function (FtsH-LoF) leads to metabolic changes. Alamar blue assay measuring reductive metabolism of the FtsH-LoF strains. Larger relative fluorescence units (RFU) values indicate higher activity of metabolic reduction. Fluorescence measured for (a) strains containing the pP_{srtA} vectors ($t = 18$ h), and (b) strains containing the pP_{nisA} vectors ($t = 3$ h) post Alamar blue incubation. The reduced incubation time for strains in (b) is due to their tendency for fluorescence saturation at longer incubation times. Antibiotic selection and nisin induction were present throughout incubation with the Alamar blue reagent. Error bars represent the standard error of mean from three biological replicates. Tukey's test for ANOVA. $^{****}p < 0.0001$. (c–e) Extracellular acidification rate (ECAR) quantified from *ftsH* loss-of-function strains using the Agilent Seahorse assay as an indirect measure of glycolysis. Error bars represent the standard error of mean from four biological replicates. Constructs in pP_{nisA} plasmids are under a nisin inducible promoter induced with 25 ng/mL nisin, while pP_{srtA} plasmids are under a constitutive promoter. Dunnett's test for ANOVA. $^{*}p < 0.05$; $^{**}p < 0.01$; $^{***}p < 0.001$; $^{****}p < 0.0001$.

similarly shows that Δ*mprF1* Δ*mprF2 ftsH*(G37X) displays a slower evolution to resistance as compared to the Δ*mprF1* Δ*mprF2* passage control. Hence, these data suggest that the slowed evolution is not due solely to greater DAP sensitivity and initial HGPC at Day 1 and suggest that other contributing factors might be at play. This slowed evolution, however, cannot be explained by differences in mutation

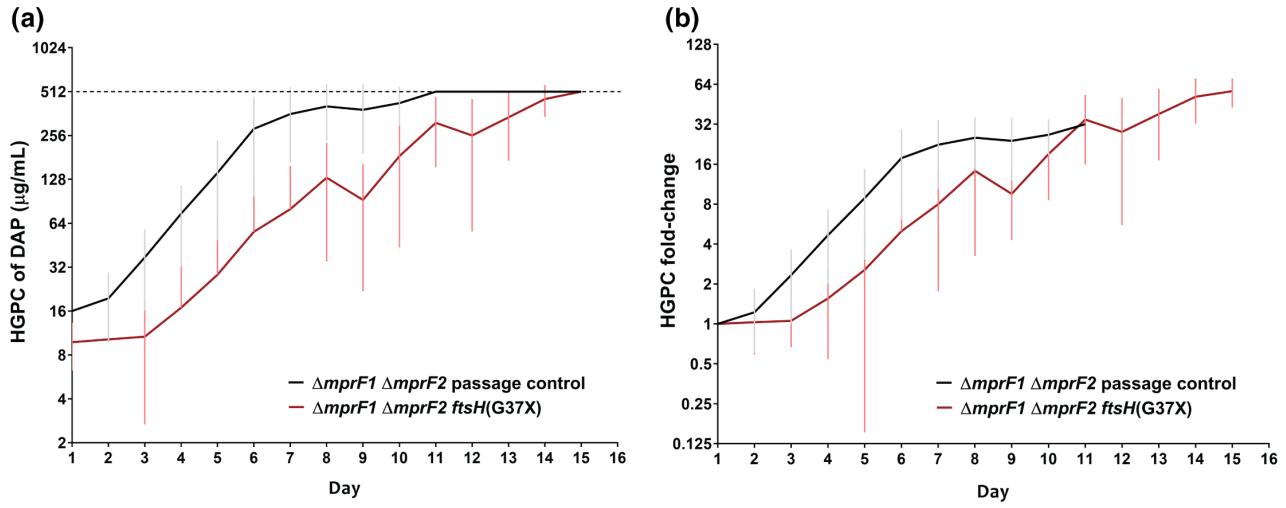

(c)

Mutation rate		
Strain	**Mean mutation rate**	**Adjusted p-values**
Δ*mprF1* Δ*mprF2* passage control	$7.75 \times 10^{-10} \pm 7.83 \times 10^{-11}$	-
Δ*mprF1* Δ*mprF2 ftsH*(G37X)	$1.31 \times 10^{-9} \pm 3.90 \times 10^{-11}$	< 0.001

FIGURE 4 FtsH-LoF slows speed of evolution to DAP^R and increases basal mutation rates in the Δ*mprF1* Δ*mprF2*. (a) Mean highest growth permissive concentration (HGPC) of DAP across time from in vitro evolution of Δ*mprF1* Δ*mprF2 ftsH*(G37X) and Δ*mprF1* ΔmprF2 passage control to DAP^R of HGPC of 512 μg/mL DAP. (b) Fold-change of HGPC across time of (a), to take into account and to correct for the difference in starting HGPC. Error bars indicate standard deviation from nine parallel lines of evolution. (c) Mean mutation rate with standard deviation of *mprF* mutants from three replicates from independent experiments assayed by the Luria–Delbrück fluctuation assay which measures phenotypic mutation rates. The comparison was made between Δ*mprF1* ΔmprF2 passage control against Δ*mprF1* Δ*mprF2 ftsH*(G37X). Significance tested by permutation (10,000 shuffles within experimental groups to preserve the integrity of the experimental design).

rate where intriguingly we observe a significant increase in mutation rate in Δ*mprF1* Δ*mprF2 ftsH*(G37X) as compared to the Δ*mprF1* Δ*mprF2* passage control (Figure 4c).

To determine whether any unique mutations were acquired under FtsH-LoF, end point DAP^R Δ*mprF1* Δ*mprF2 ftsH*(G37X) isolates were sequenced. Similar mutations were detected in both Δ*mprF1* Δ*mprF2* and Δ*mprF1* Δ*mprF2 ftsH*(G37X) DAP^R isolates including *cls1*, *cls2*, *liaX*, and RS09725 (File S1d). Mutations in *liaF* which are also closely linked to DAP^R in *Enterococci*, as well as in *rpoC* that are associated with DAP^R in *S. aureus* were also observed only in the Δ*mprF1* Δ*mprF2 ftsH*(G37X) DAP^R isolates (Arias et al., 2011; Miller et al., 2016). Mutations in other genes and intergenic regions were also observed only in the Δ*mprF1* Δ*mprF2 ftsH*(G37X) DAP^R isolates, but whether they are associated with DAP^R or are just spontaneous mutations have yet to be determined (File S1d).

2.5 | Proteomic investigation of FtsH-LoF reveals *hrcA* as a key driver of slowed evolution

To determine the mechanisms underlying the slowed evolution and growth phenotypes following introduction of *ftsH*(G37X) to the *mprF* mutant background, we investigated the proteomic consequence of FtsH-LoF in the wild-type background, by conducting peptide mass spectrometry on the whole cell lysates and membrane fractions of wild-type pMSP3535-6his-*ftsH* and wild-type pMSP3535-6his-*ftsH*(H456Y) following overnight induction with nisin. This experiment was performed in wild-type genetic background, instead of using the Δ*mprF1* Δ*mprF2* and Δ*mprF1* Δ*mprF2 ftsH*(G37X) strains, to enable investigation of the growth phenotypes in tandem with the slowed evolution phenotype of FtsH-LoF. Proteomic changes common between the whole cell lysates and membrane were shortlisted, and proteomic changes that could be explained by transcriptomic differences were filtered out (Table 2). From this short list, we identified several proteins that were depleted following FtsH-LoF (Table 2), which may be explained by compensatory activity of other proteases such as the Clp protease, which was transcriptionally induced when FtsH was non-functional (Log_2FC for *clpP* = 1.63; *clpE* = 1.34; *clpB* = 1.24, *clpC* = 1.15) (File S1c). Of the four proteins that accumulated in the FtsH-LoF strain (Table 2), ArcB and a putative amidase (RS02510) were shown to be likely substrates of FtsH by assessing protein stability and FtsH-dependent degradation under FtsH-LoF (Figure S3).

We hypothesized that the accumulation or depletion of these proteins might explain the slowed growth observed from FtsH-LoF

TABLE 2 Proteomic changes in FtsH-LoF (wild-type p6his-FtsH(H456Y))[a].

Gene	Gene number (new; old ID)	Identity	Proteomic log_2FC	RNAseq log_2FC
Depleted proteins				
yckE	RS05275; OG1RF_11014	Beta-glucosidase	−2.77	-
lysS	RS01060; OG1RF_10212	Lysine-tRNA ligase	−2.69	-
pyrB	RS07365; OG1RF_11430	Aspartate carbamoyltransferase	−2.54	-
lutA	RS04635; OG1RF_10886	Putative lactate utilization Fe-S protein; homologous to *B. subtilis lutA*	−2.01	1.22
gelE	RS07835; OG1RF_11526	Gelatinase E	−1.95	-
trePP	RS12410; OG1RF_12425	Glycosyl hydrolase	−1.86	-
carB	RS07350; OG1RF_11427	Carbamoyl-phosphate synthase large subunit	−1.69	0.67
cryZ	RS07135; OG1RF_11383	Putative NADPH:quinone reductase	−1.67	-
hrcA	RS05580; OG1RF_11076	Heat-inducible transcription repressor HrcA	−1.56	-
Accumulated proteins				
arcB	RS00500; OG1RF_10100	Ornithine carbamoyltransferase	2.53	−0.89
RS08610	RS08610; OG1RF_11679	Metal ABC transporter substrate-binding protein	1.14	−1.59
cls1	RS01975; OG1RF_10364	Cardiolipin synthase 1	2.46	-
RS02510	RS02510; OG1RF_10473	Amidase	2.36	-

[a]Proteomic changes that are not correlated with transcriptomic differences are displayed. Short list of proteomic changes, which are common across membrane fractions and whole cell lysates. Refer to File S1e,f for full list of proteomic changes in membrane fractions and whole cell lysates respectively. Refer to File S1c for RNAseq data that was used to filter proteomic changes that were correlated with transcriptomic expression changes.

in the wild-type. We examined each of the depleted proteins either with transposon mutants (*yckE*::Tn, *lutA*::Tn, *gelE*::Tn, *trePP*::Tn, *carB*::Tn, *cryZ*::Tn, *hrcA*::Tn) (Kristich et al., 2008) or by CRISPRi silencing of genes for depleted proteins that were not available in the transposon library (*lysS* and *pyrB*) (Afonina et al., 2020). To mimic accumulation of proteins, *arcB*, RS08610, *cls1* and RS02510 were cloned into a nisin inducible plasmid for induced overexpression. This panel of mutants was assayed for growth and we observed that *trePP*::Tn, *lysS* silencing, and overexpression of RS02510 resulted in slowed growth, indicating that these gene products could be contributing to the growth defect observed in a wild type genetic background with FtsH-LoF (Figure S4a–f).

We next subjected the same panel of transposon mutants to in vitro evolution to DAP^R to determine their contribution to the slowed evolution in Δ*mprF1* Δ*mprF2 ftsH*(G37X). However, in the initial evolution assay, all strains had a similar profile as wild-type where the HGPC of every strain was saturated at the assay's upper selection limit (2X HGPC) for most of the assay making it hard to distinguish any difference between the strains (data not shown). To overcome this limitation, evolution was performed at an expanded DAP selection range of 0.5X, 1X, 2X, 4X, 8X HGPC instead. We observed that only *hrcA*::Tn was significantly associated with slowed evolution when observing the progression of both HGPC, and HGPC fold-change over time (Figure 5a,b). However, when we calculated mutations rates, we found that *hrcA*::Tn was similar to wild-type (Figure 5c). Of the remaining transposon mutants, most displayed similar evolution profiles as the wild-type in terms of both HGPC and HGPC fold-change over time (Figure S5). The slight delay observed for *lutA*::Tn (lactate utilization protein) was due to a single outlier that evolved much slower than the rest (Figure S5a). Evolution of CRISPRi and overexpression mutants was not possible, due to plasmid insert loss during evolution despite maintenance of antibiotic selection pressure (data not shown). Hence, *hrcA* appears to play a major contributing role toward the slowed evolution in FtsH-LoF.

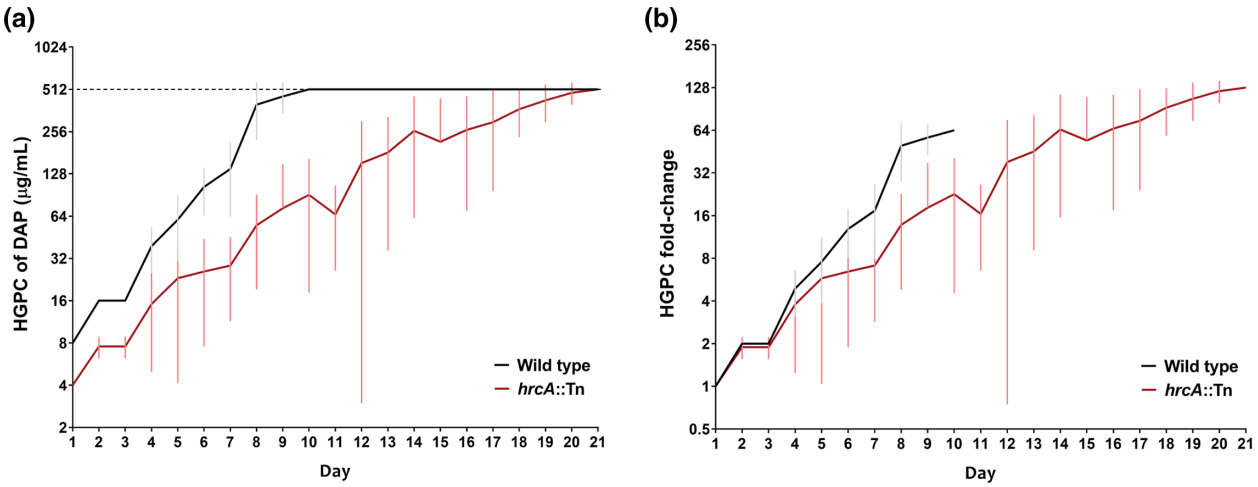

(c)

Mutation rate of mutants		
Mutant	**Mean mutation rate**	**Adjusted p-values**
Wild type	$3.76 \times 10^{-9} \pm 2.53 \times 10^{-9}$	-
hrcA::Tn	$2.41 \times 10^{-9} \pm 2.03 \times 10^{-9}$	0.245

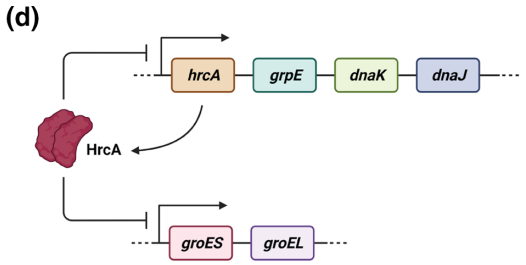

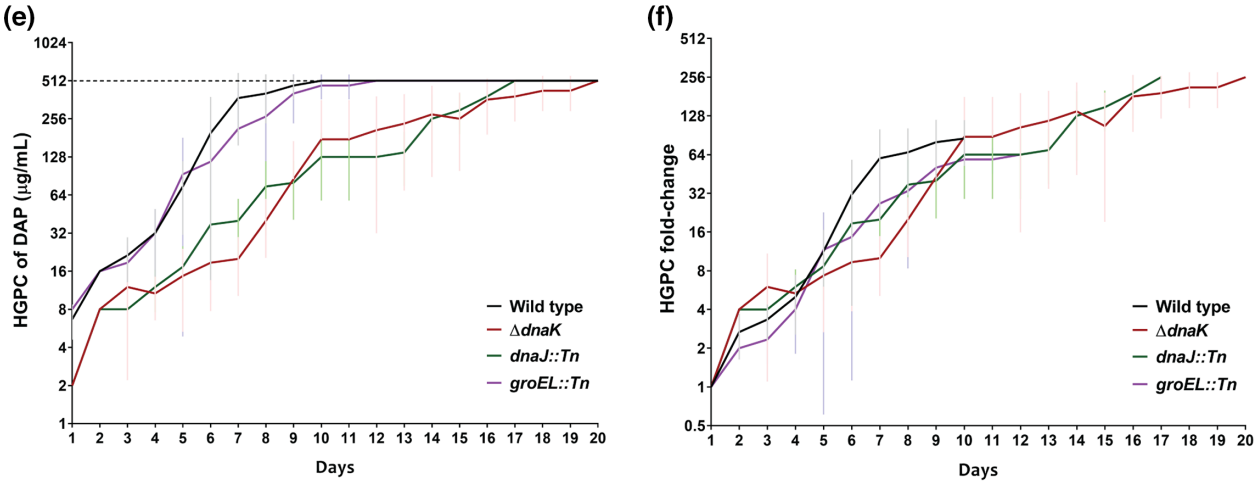

(g)

Mutation rate of mutants		
Mutant	**Mean mutation rate**	**Adjusted p-values**
Wild type	$1.27 \times 10^{-8} \pm 1.68 \times 10^{-8}$	-
dnaJ::Tn	$3.36 \times 10^{-9} \pm 3.82 \times 10^{-9}$	0.601
Δ*dnaK*	$6.60 \times 10^{-9} \pm 7.05 \times 10^{-9}$	0.601
groEL::Tn	$1.84 \times 10^{-8} \pm 2.20 \times 10^{-8}$	0.601

FIGURE 5 Disruption of HrcA and its target regulatory chaperones alters speed of DAP^R acquisition. Mean highest growth permissive concentration (HGPC) of DAP across time from in vitro evolution to DAP^R (HGPC of 512 μg/mL DAP) and corresponding fold-change of HGPC across time for (a, b) *hrcA*::Tn, and (e, f) chaperone mutants—Δ*dnaK*, *dnaJ*::Tn, *groEL*::Tn. Error bars indicate standard deviation from nine parallel lines of evolution for (a, b) and six parallel lines of evolution for (e, f). Evolution was performed using an expanded antibiotic selection range of 0.5X, 1X, 2X, 4X, 8X HGPC instead. (d) Model of the HrcA regulon, where HrcA negatively regulates the *hrcA-grpE-dnaK-dnaJ* and *groES-groEL* operons. Created with BioRender.com. (c, g) Mean mutation rate with standard deviation of *mprF* mutants from three replicates from independent experiments assayed by the Luria-Delbrück fluctuation assay which measures phenotypic mutation rates. Comparisons were made for each mutant against the wild-type. Significance tested by permutation (10,000 shuffles within experimental groups to preserve the integrity of the experimental design) with Benjamini–Hochberg adjusted *p*-values to control false discovery in multiple comparisons.

2.6 | Chaperones downstream of the *hrcA* regulon alter evolution speeds

HrcA is a transcriptional repressor of chaperone operons—*hrcA-grpE-dnaK-dnaJ* and *groES-groEL*—where it binds the conserved controlling inverted repeat of chaperone expression (CIRCE) element upstream of these operons (Schumann, 2016) (Figure 5d). From transcriptomic data of FtsH-LoF in the wild-type background, we indeed observed upregulation of *grpE*, *dnaK*, and *groEL* (Log_2FC of 1.13, 1.53, 1.58 respectively) in concert with the depletion of HrcA (File S1c). Hence, we reasoned that the depletion of HrcA could relieve transcriptional repression of these downstream chaperones, which could be contributing to the altered DAP^R evolution speeds. *dnaJ*::Tn, Δ*dnaK* and *groEL*::Tn were subjected to in vitro evolution using the same expanded DAP selection range as HGPC saturation at the upper limit of the assay occurred as described above (data not shown). We hypothesized that under FtsH-LoF, reduction of the repressor HrcA would result in upregulation of chaperones resulting in slowed evolution. Conversely, we expect that the loss of chaperone activity will result in a quickened evolution process.

However, unexpectedly, *groEL*::Tn displayed similar evolution profiles as the wild-type strain, while evolution of *dnaJ*::Tn and Δ*dnaK* were slowed when comparing DAP HGPC over time (Figure 5e). However, when accounting for the increased DAP-sensitivity of *dnaJ*::Tn and Δ*dnaK* strains, with twofold lower DAP MIC than the wild-type (Table 1) by comparing HGPC fold-change over time, we observed that Δ*dnaK* strongly slows progression to DAP^R, whereas *dnaJ*::Tn and *groEL*::Tn had a modest impact on evolution time (Figure 5f). These differences similarly cannot be explained by changes in mutation rate as they were similar across the strains tested (Figure 5g). Although we did not further investigate *grpE* and *groES*, we can expect evolution speeds to be similar to mutants of *dnaK* and *dnaJ*, and *groEL* respectively, since GrpE functions as a co-chaperone together with DnaK and DnaJ, while GroES and GroEL are co-chaperones that function together in the same complex (Harrison, 2003; Hayer-Hartl et al., 2016). While the *hcrA*-regulated chaperones that we tested displayed opposing phenotypes to what was expected, we speculate that their combined effects together with other HrcA-regulated genes result in the observed slowed evolution in loss of *hrcA*.

Since most of the strains that we observed slowed evolution to DAP^R have increased DAP-sensitivity, it was plausible that increased DAP-sensitivity could be predictive of slowed evolution. To investigate this, we assayed mutants of the LiaFSR three-component system and cardiolipin synthase, which were previously shown to be more DAP-sensitive and are directly linked to DAP^R (Arias et al., 2011; Miller et al., 2013). Δ*liaR*, Δ*liaFSR*, and *cls1*::Tn Δ*cls2*, which display 2- to 16-fold lower DAP MIC than the wild-type, were evolved to DAP^R (Table 1). Due to the drastically lowered initial DAP HGPC, Δ*liaR* and Δ*liaFSR* displayed slower HGPC progression over time while *cls1*::Tn Δ*cls2* displayed a similar profile to the wild-type (Figure S6a). However, when considering the HGCP fold-change over time, surprisingly Δ*liaR* and Δ*liaFSR* displayed a much faster rate of evolution as compared to the wild-type strain while *cls1*::Tn Δ*cls2* was largely to wild-type (Figure S6b). Hence, increased DAP-sensitivity does not always correlate with, nor does it predict, slower evolution to DAP^R.

3 | DISCUSSION

Treatment of Enterococcal infections has become increasingly challenging with the rise of antimicrobial resistance, including resistance to daptomycin, which is one of the drugs of last resort used to treat drug resistant infections such as vancomycin-resistant Enterococci (Patel & Gallagher, 2015). With *E. faecalis* contributing to the majority of Enterococcal infections, there is increasing interest to elucidate the factors driving DAP^R in this species (Pfaller et al., 2019). Through a combination of in vitro evolution assays and sequencing of DAP^R isolates, previous efforts have revealed membrane remodeling, antimicrobial stress sensing, oxidative stress response, and drug efflux to contribute to DAP^R (Arias et al., 2011; Khan et al., 2019; Miller et al., 2013; Mishra et al., 2012; Tran et al., 2015; Tran, Panesso, Mishra, et al., 2013).

However, less focus has been placed on factors affecting the speed of antibiotic resistance evolution, especially in the case of DAP^R where slowing resistance acquisition could inform anti-resistance strategies. Factors that broadly affect the propensity to evolve resistance to antibiotics have been well-described. These factors influence antibiotic resistance evolution through DNA-repair machinery and stress response pathways, including the DNA-damage-associated SOS-response, error-prone DNA polymerases, sigma factors, and the DNA translocase Mfd (Al Mamun et al., 2012; Boshoff et al., 2003; Erill et al., 2007; Merrikh & Kohli, 2020; Ragheb et al., 2019). Additionally, chaperones also provide buffering capacity for the fitness cost of resistance mutations affecting protein stability (Aguilar-Rodríguez et al., 2016; Fay et al., 2021). Other than these general factors, there are others that specifically influence the evolution to DAP^R. Recently, *liaFSR* was reported to affect the speed of DAP^R evolution in *E. faecium*, where deletion of *liaR* significantly slows evolution suggesting that LiaFSR activation is the dominant pathway to DAP^R in *E. faecium* (Prater et al., 2021). A synergistic effect of DAP with another antibiotic has also been reported to delay DAP^R acquisition where the co-administration of DAP with fosfomycin in *S. aureus* delayed the evolution to DAP^R (Mishra et al., 2022). While some information on factors affecting evolution to DAP^R exist, there is still limited mechanistic understanding at a genetic level for DAP^R acquisition in *Enterococci*.

Apart from the few well-described mechanisms of DAP^R in *E. faecalis*, here we report that the multiple peptide resistance factor (MprF) also plays some role in DAP^R where the loss of *mprF2* hypersensitizes the already DAP-sensitive OG1RF strain by further decreasing DAP MIC. Through in vitro evolution of the *mprF* mutants to DAP^R to uncover novel mutations that might be otherwise masked by *mprF* activity, we discovered that evolution was slowed considerably in Δ*mprF1* Δ*mprF2*. Apart from this, by utilizing mutants of *mprF*,

we unmasked loss-of-function mutations (LoF) in *ftsH* observed only within the Δ*mprF1* Δ*mprF2* genetic background early in evolution (Figures 1d and 2a).

The effect of chaperones on accelerating protein evolution is well-documented and is likely the reason for the observed slowed evolution in their absence. The DnaK chaperone can provide mutational robustness by buffering deleterious mutations that affect protein structure and function and has been described to buffer the fitness cost of mutations associated with rifampicin resistance in *Mycobacteria* (Aguilar-Rodríguez et al., 2016, Fay et al., 2021). A similar mechanism might be at play in *E. faecalis* such that loss of *dnaK* leads to slowed resistance evolution due to reduced ability to buffer mutations that affect protein stability. DnaK has also been implicated in central metabolism and carbon source utilization in *E. coli* (Anglès et al., 2017). This could similarly be the case for *E. faecalis*, since we observed metabolic changes in terms of altered ability for extracellular acidification and metabolic reduction in the FtsH-LoF mutants where chaperones are upregulated (Figure 3; File S1c). DnaK and its co-chaperone DnaJ might also be essential in relieving *E. faecalis* of metabolic constraints that might be introduced by mutations accumulated through evolution.

Under FtsH-LoF, the resulting depletion of HrcA results in slowed evolution to DAP^R. With HrcA being a chaperone operon repressor, it is expected that its depletion results in upregulation of downstream chaperones that contribute to this slowed evolution. Conversely, we would expect that disruption of these chaperones would enhance evolution instead. Unexpectedly, we instead observed slowed evolution when the chaperone DnaK was disrupted, and to a lesser extent, when DnaJ and GroEL were disrupted. Hence at present, we do not yet fully understand how the depletion of HrcA enhances DAP^R evolution. One possibility is that by using the reductive approach in deleting or disrupting individual chaperones, we are only probing their individual contribution to resistance evolution, which may not reflect the FtsH-LoF environment where multiple chaperones are upregulated under HrcA depletion. Furthermore, given that chaperones are canonically known to promote evolution by stabilizing deleterious mutations in proteins, it is unlikely that they are the sole reason behind the slowed evolution under HrcA depletion. It is more likely that the involvement of chaperones in combination with other *E. faecalis* genes regulated by HrcA together result in the slowed evolution under HrcA depletion, which is a topic for further investigation.

Additionally, HrcA depletion is unlikely to be the sole reason for the observed slowed evolution under FtsH-LoF since Δ*mprF1* Δ*mprF2* *ftsH*(G37X) displayed higher mutation rates and this was not observed for *hrcA*::Tn. It is possible that the other accumulated proteins under FtsH-LoF might also play a role in influencing evolution, but we were unable to investigate further due to plasmid stability limitations in mimicking overexpression during in vitro evolution (Table 2). Additionally, with FtsH-LoF, there is a consequent decrease in HrcA, suggesting compensatory activation or upregulation of other proteases such as Clp that result in HrcA depletion. Another open question is the identity of these compensatory proteases that are responsible for HrcA depletion in FtsH-LoF. Nonetheless, our study provides evidence of the involvement of *ftsH* and *hrcA* in *E. faecalis* DAP^R evolution that has not been previously described and presents them as potential targets for means of influencing evolution rates and anti-resistance strategies. We also provide evidence of an alternative route to DAP^R involving protein quality control and chaperone regulation, apart from the well-described routes involving antimicrobial stress sensing and membrane remodeling.

Furthermore, we also discovered that differences in mutation rates and DAP-sensitivity of strains is not an accurate predictor of evolution profiles and speed of evolution to DAP^R. This is exemplified by the case of Δ*mprF1* Δ*mprF2* *ftsH*(G37X), which displayed a significantly higher mutation rate as compared to the parental control, and yet evolved at a much slower speed; as well as Δ*liaR* and Δ*liaFSR*, which displayed close to 16-fold lower MIC than the wild-type, and yet were able to evolve faster to DAP^R based on fold-change of DAP HGPC over time. It is possible in these cases that chaperone involvement, stress response systems, or other factors could be at play. Hence, it is important that assumptions on a strain's propensity to evolve resistance should not be solely made based on mutation rate and MIC information, and that direct investigation of evolution profiles be empirically evaluated.

Our study also revealed that FtsH is essential in the wild-type background but is dispensable in Δ*mprF1* Δ*mprF2*. Several proteins that were depleted or accumulated under FtsH-LoF could explain the reason for the slowed growth in the wild-type, namely the depletion of TrePP, LysS, and accumulation of a putative amidase (RS02510). Since TrePP is a glycosyl hydrolase responsible for the hydrolysis of glycosidic bonds, particularly that of trehalose-6-phosphate, and lysine-tRNA ligase is responsible for the ligation of lysine to tRNA, it is possible that reduced ability to break down complex sugars and produce essential lysine-tRNA could be contributing to the growth defect. Furthermore, the absence of MprF that utilizes lysine-tRNA as a substrate in Δ*mprF1* Δ*mprF2* could reduce the pressure of a limited lysine-tRNA pool allowing for normal growth under FtsH-LoF. Related to the growth defect, the accumulation of the putative amidase (RS02510) could also be contributing to the slowed growth, especially since amidases tend to play roles in cell division where they hydrolyze crosslinked peptidoglycan to allow for septation, dysregulation of this putative amidase could have similar effects (Do et al., 2020; Vollmer et al., 2008). Apart from growth-related observations, FtsH-LoF in the wild-type also resulted in a significant increase in cell chaining, which could be mediated by the depletion of gelatinase E (GelE) under FtsH-LoF. Since gelatinases act to cleave autolysin to process it into its active form, the reduction in gelatinase E likely results in reduced autolysin activity resulting in dysfunctional cell division and increased cell chaining (Stinemetz et al., 2017). Furthermore, we have also shown that ArcB and RS02510 are substrates of FtsH, providing the first identification of FtsH substrates in *E. faecalis*. Therefore, while *ftsH* loss is tolerated in Δ*mprF1* Δ*mprF2*, it is essential in the wild-type, where its loss leads to a growth defect driven by altered metabolism and altered cell division.

The reason behind the synthetic viability of FtsH-LoF in Δ*mprF1* Δ*mprF2* is still not fully understood. Given the altered lipidomic and metabolic landscape of Δ*mprF1* Δ*mprF2* (Rashid et al., 2023), it is possible that this would provide a permissive environment to offset the deleterious effects of FtsH-LoF. This could be mediated through glycosyl hydrolase (TrePP), where its disruption causes growth defects in the wild-type and is depleted in FtsH-LoF. However, TrePP is transcriptionally up-regulated in Δ*mprF1* Δ*mprF2*, possibility compensating for the TrePP loss under FtsH-LoF (Rashid et al., 2023). While not known to affect growth, transcriptional and proteomic expression of *mprF2* was also increased in FtsH-LoF (Log_2FC *mprF2* = 0.54, MprF2 = 2.59), which could be off-set by *mprF2* deletion in Δ*mprF1* Δ*mprF2*. While the picture is not yet complete, these findings hint toward an altered metabolic environment within Δ*mprF1* Δ*mprF2*, which is an avenue for future investigation.

It is also important to note that while this study focuses on protein abundance and gene expression to guide investigation and data interpretation, protein localization and stability have yet to be considered. It is possible that contributing factors influencing both synthetic viability of FtsH-LoF in Δ*mprF1* Δ*mprF2* and progression to DAP^R could associated with delocalization of important proteins that might have been missed with our current methodology that only takes into account protein abundance and gene expression levels. This is especially relevant since the Δ*mprF1* Δ*mprF2* strain is known to possess a drastically altered lipidome, which could hint to possible alterations in membrane microdomain organization and consequent protein localization (Rashid et al., 2023). Membrane microdomains are domains of different lipid composition within the cell membrane where cellular processes are organized (Barák & Muchová, 2013; Lopez & Koch, 2017). For instance, PBP2a in *S. aureus*, which is involved in β-lactam resistance, is organized within membrane microdomains that if disrupted, fail to properly oligomerize and consequently leads to enhanced antibiotic sensitivity (García-Fernández et al., 2017). Hence, it is not implausible to hypothesize that a similar phenomenon could be occurring in our system as well, which presents an intriguing direction for future investigation. Additionally, it is important to acknowledge that some of the mutants used in this study are transposon mutants, and there is a formal possibility that polar effects of the transposon insertions might also be contributing to observed phenotypes. Ideally, unmarked chromosomal deletion mutants should be used in future investigations.

Taken together, we have demonstrated that FtsH is essential in wild-type *E. faecalis*, but loss of function is permissible in Δ*mprF1* Δ*mprF2*, which slows DAP^R evolution through the indirect depletion of HrcA and subsequent changes in regulatory flux of the downstream chaperone operons (Figure 6). Under FtsH-LoF in the wild-type background, the ability for metabolic reduction and extracellular acidification is reduced along with FtsH-LoF-associated changes in TrePP, LysS and amidase levels resulting in growth impairment. Whereas in FtsH-LoF in Δ*mprF1* Δ*mprF2*, growth is not affected, instead, HrcA is indirectly depleted by compensatory action of other proteases. While the loss of HrcA results in slowed evolution, the contribution of downstream genes in the regulon, *dnaK*, *dnaJ*, and *groEL* does not fully explain the cause. It is likely that there is more complex higher-order regulation present involving other genes that results in a net decrease in evolution speeds. This study provides the first major characterization of FtsH both in terms of its substrates and its functional role in *E. faecalis* involving growth and metabolism, as well as the previously undescribed involvement in antibiotic resistance and resistance acquisition. The possibility of manipulating DAP^R evolution by targeting FtsH, HrcA and chaperone presents an enticing opportunity for their utility as both a research tool and as possible candidates for development of anti-resistance strategies. This is especially the case for FtsH where its essentiality further highlights its potential as a therapeutic target.

3.1 | Experimental procedures

Strains, growth conditions, growth kinetics, live/dead staining, RNA sequencing, and cloning methods are detailed in supplementary text.

3.2 | In vitro evolution of *E. faecalis* to daptomycin resistance

The protocol was adapted from a previously published in vitro evolution experiment done in *E. faecalis* V583 (Palmer et al., 2011). For each strain, multiple parallel lines of evolution experiment were performed. First, 100X dilutions of overnight bacterial cultures of each strain were made in BHI supplemented with 1.25 mM calcium chloride (Sigma, USA) (50 mg L^{-1} Ca^{2+}) containing daptomycin (DAP) (Gold Biotechnology, USA) concentrations of 1X MIC, 2X MIC and 4X MIC, and incubated at 37°C in static conditions for 22 to 26 h. Cultures of every evolution line were examined for visible bacterial growth. Bacterial cultures at the highest growth-permissive concentrations (HGPCs) are diluted 100X into fresh DAP-containing medium at 0.5X, 1X and 2X HGPC. This was repeated until HGPC of 512 μg/mL was achieved. Bacterial cultures were then passaged in plain BHI broth for 3 days to obtain stable mutants. Isolates were glycerol stocked each day in 25% v/v glycerol. Refer to Figure S7 for the schematic of the in vitro evolution workflow. In instances where evolution profiles of the tested strains are consistently at the 2X HGCP and are saturated at the upper HGPC limit of the assay, an expanded range of 0.5X, 1X, 2X, 4X and 8X HGCP is used for selection instead.

3.3 | Whole-genome sequencing

Whole-genome sequencing was conducted on the glycerol stocked DAP^R isolates from the wild type, Δ*mprF1*, Δ*mprF2*, Δ*mprF1* Δ*mprF2*, and Δ*mprF1* Δ*mprF2 ftsH*(G37X) backgrounds. Genomic DNA was extracted from overnight bacterial cultures using PureLink Genomic DNA Mini Kit (Thermo Fisher Scientific). Library preparation using MiSeq reagent kit v3 and whole-genome sequencing using MiSeq was

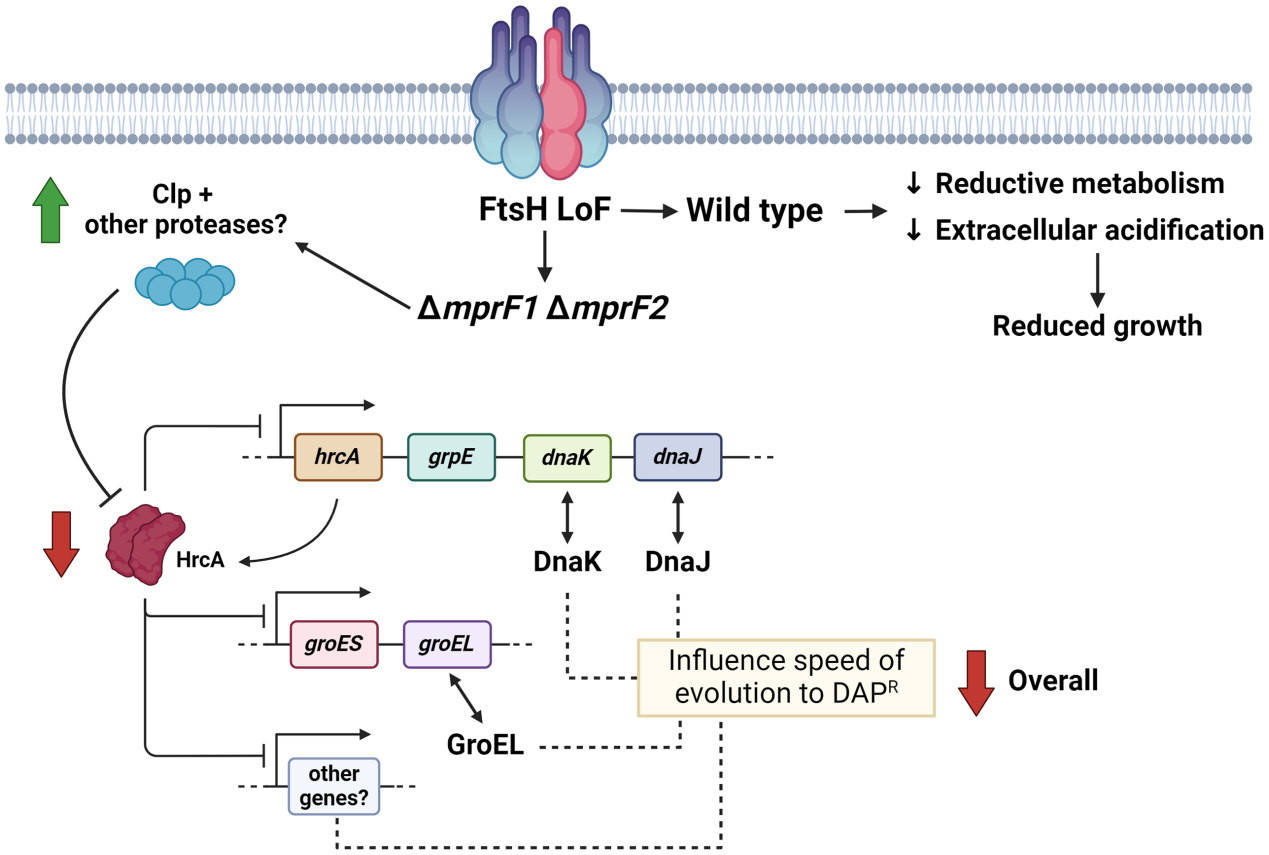

FIGURE 6 Model of FtsH's influence on speed of DAP^R evolution and reduced growth in the wildtype. FtsH loss of function (LoF) indirectly leads to an increase in the Clp protease. This along with other proteases likely results in depletion of HrcA, which relieves repression of the chaperone operons (*hrcA-grpE-dnaK-dnaJ* and *groES-groEL*). Further investigation revealed that *dnaK*, *dnaJ* influence the speed of DAP^R evolution. This combined with the extended regulatory effects of *hrcA* on other genes likely results in an overall combined effect of decreased evolution speed. FtsH-LoF also results in metabolic changes such as decreased ability for acidification and reductive metabolism that could be partly responsible for the reduced growth in the wild-type. Created with BioRender.com.

done by the sequencing facility of Singapore Centre of Life Science Engineering (SCELSE, Singapore). Library preparation using HiSeq reagent kit and whole-genome sequencing using HiSeq X was done for Δ*mprF1* Δ*mprF2 ftsH*(G37X) DAP^R isolates by SCELSE sequencing facility. Data were analyzed using CLC Genomics Workbench 8.0. The complete OG1RF reference genome (NC_017316) from NCBI database was used for mapping and annotation. The threshold variant frequency was set as 35%. Non-synonymous mutations within coding regions were filtered for. All structural variations were manually confirmed on the mapping track.

3.4 | Minimal inhibitory concentration (MIC) by microplate dilution

Stationary phase cultures to be tested were grown until mid-log phase and normalized to OD_{600} of 0.7. MIC assays were performed in a 96-well plate as described previously (Wiegand et al., 2008), with the following modifications. Antibiotics were diluted in BHI or MHB II media supplemented with 1.25 mM calcium chloride (50 mg L^{-1} Ca^{2+}), in 2-fold dilutions, from 256.0 μg/mL to 0.5 μg/mL of daptomycin. Cultures with daptomycin were incubated for 16–18 h at 37°C in static conditions before assessing for growth in the wells to estimate the MIC.

3.5 | RNA sequencing

Sequencing of RNA was done from wild-type pMSP3535-6his-*ftsH*(H456Y) and wild-type pMSP3535-*ftsH*(H456Y). Detailed methods are described in the supplementary text file.

3.6 | FtsH proteomic analysis

Wild-type pMSP3535-6his-*ftsH*(H456Y) and wild-type pMSP3535-*ftsH*(H456Y) strains were grown to mid-log phase and induced for expression of their respective plasmids' gene constructs with 125 ng/mL of nisin for 16–18 h at 37°C in static conditions and cell pellets were harvested. The membrane fraction was isolated from the harvested pellets as previously described, resuspended with 100 μL of 50 mM Tris–HCl, pH 8.0, and boiled with 33.3 μL of

NuPAGE® LDS Sample Buffer (4X) (Thermofisher, USA) and 10 μL of 1 M DTT (Maddalo et al., 2011). Samples were then run on SDS-PAGE on a 4–12% NuPAGE® Bis-Tris mini gel in a XCell SureLock® Mini-Cell filled with MES SDS running buffer (Invitrogen, USA) until samples just entered the gel. Gels were then silver-stained by fixing with 50% v/v methanol and 5% v/v acetic acid solution, sensitizing with 0.02% w/v sodium thiosulfate solution, silver-stained with 0.1% w/v silver nitrate and 3% v/v formalin solution and developed using 2% w/v sodium carbonate and 1.5% v/v formalin solution. The concentrated protein band of each lane was excised and stored in Eppendorf tubes filled with water. Samples were then sent to the Taplin Mass Spectrometry Facility, Harvard Medical School, Boston, Massachusetts, USA, for peptide mass spectrometry and proteomic analysis. Peptide counts were normalized using tweeDEseq (TMM normalization) and statistics were done using Reproducibility-Optimized Test Statistic (ROTS) (Esnaola et al., 2013; Suomi et al., 2017).

3.7 | Mutation rate assay (Luria-Delbrück fluctuation assay)

Overnight stationary phase cultures were diluted 10, 000X in 40 mL of BHI supplemented with 1.25 mM calcium chloride (50 mg L^{-1} Ca^{2+}). 100 μL of diluted culture was then added into each well of a 96-well microtiter plate, sealed and incubated at 37°C in static conditions for 16–18 h. 24 wells from the plate were pooled followed by serial dilution and plating on non-selective BHI agar plate for CFU enumeration. This determines the average cell number (N). Whole volumes (100 μL) of each of the 72 wells/cultures were then transferred into wells of a 24-well microtiter plate containing 900 μL BHI supplemented with 1.25 mM calcium chloride and daptomycin (dilution was taken into account such that final daptomycin concentration is 3X MIC). Plates were incubated at 37°C in static conditions and observed for growth visually by the presence of turbid wells for up to 7 days. The fraction of wells/cultures with zero growth indicating zero mutant cells is defined as p_0. The expected number of mutation events per culture (m) is calculated as, $m = -\ln(p_0)$. The mutation rate (μ) is calculated as: $= \frac{m}{N}$.

To determine whether the differences in mutation rates between strains are statistically significant, we performed a permutation test with 10,000 iterations, shuffling data within each experimental group to preserve the integrity of the experimental design. The *p*-values were adjusted using the Benjamini–Hochberg method to control the false discovery rate (Benjamini & Hochberg, 1995; Good, 2013).

3.8 | Alamar blue assay

Overnight cultures were normalized to OD_{600} 0.5 in PBS and diluted 1:10. The ability to reduce the resazurin dye was measured using the AlamarBlue™ HS cell viability reagent (Thermoscientific, USA) according to the manufacturer's instructions. Antibiotic selection and nisin induction at 25 ng/mL nisin where required were maintained throughout the incubation period with the Alamar Blue reagent. Fluorescence was measured at 18 hours post incubation for strains containing the pP_{srtA} vectors, and 3 hours of postincubation for strains containing pP_{nisA} vectors. The shortened incubation time for strains containing pP_{nisA} vectors is due to the tendency for the fluorescence signal to saturate at 18 hours when antibiotic selection and nisin induction are present.

3.9 | Seahorse assay

Mid-log phase cultures were washed once and normalized to OD_{600} 0.7 in BHI. Cultures were then added to a Cell-Tak™ Cell and Tissue Adhesive (Corning, USA) coated XF96 cell culture microplate (Agilent, USA). Sterile media was added as blanks for background measurement. Microplate wells were coated with 25 μL of 22.4 μg/mL Cell-Tak™ prior to use according to the manufacturer's instructions. Plates were then centrifuged at 6000 × *g* for 15 mins to allow for cells to adhere to the bottom of the plate. A XFe96 sensor cartridge that has been soaked in calibration solution according to the manufacturer's instruction was first loaded into the Seahorse XFe96 Analyzer (Agilent, USA) for instrument calibration, followed by the microplate containing the adhered cultures. Cultures were then measured for their oxygen consumption rate (OCR) and extracellular acidification rate (ECAR) for 120 min at the following cycle settings: Mix—2 mins 30 s, Wait—0 min, Measure—4 min, no injection.

AUTHOR CONTRIBUTIONS

Kimberly A. Kline: Conceptualization; funding acquisition; project administration; supervision; writing – original draft; writing – review and editing. **Zeus Jaren Nair:** Conceptualization; methodology; investigation; supervision; writing – original draft; writing – review and editing; formal analysis; project administration. **Iris Hanxing Gao:** Conceptualization; formal analysis; investigation; methodology; writing – review and editing. **Aslam Firras:** Formal analysis; investigation; methodology; writing – review and editing. **Kelvin Kian Long Chong:** Formal analysis; investigation; methodology; writing – review and editing. **Eric D. Hill:** Formal analysis; writing – review and editing. **Pei Yi Choo:** Investigation; methodology; writing – review and editing. **Cristina Colomer-Winter:** Methodology; investigation; writing – review and editing. **Qingyan Chen:** Investigation; methodology. **Caroline Manzano:** Investigation; methodology. **Kevin Pethe:** Supervision; writing – review and editing.

ACKNOWLEDGMENTS

We thank Swaine Chen for important scientific input over the course of this project. We would like to thank Ekaterina Sviriaeva from Lee Kong Chian School of Medicine, Nanyang Technological University for access, training, and the initial consumables for the Seahorse XFe96 Analyzer. We would also like to thank Ross Tomaino from

Taplin Mass Spectrometry Facility, Harvard Medical School, Boston, Massachusetts for providing support for peptide mass spectrometry. We also extend our appreciation to Gary Dunny from University of Minnesota Medical School for providing the *E. faecalis* OG1RF transposon library, for which several mutants were used in our assays. Open access funding provided by Universite de Geneve.

This work was supported by the Singapore Centre for Environmental Life Sciences Engineering (SCELSE), funded by the National Research Foundation and Ministry of Education, Singapore under its Research Centre of Excellence Programme, as well as by the Singapore Ministry of Education under its Tier 1 program (MOE2017-T1-001-269) and the National Medical Research Council Open Fund (MOH-000645), both awarded to K.A.K. and transferred to K.P. Z.J.N. and this work was also partially supported by the National Research Foundation, Singapore, under its Campus for Research Excellence and Technological Enterprise (CREATE) program, through core funding of the Singapore-MIT Alliance for Research and Technology (SMART) Centre, Antimicrobial Resistance Interdisciplinary Research Group (AMR IRG). This work was additionally supported by funding to K.A.K. from the Société Académique de Genève and from the Swiss National Science Foundation (Schweizerischer Nationalfonds zur Förderung der Wissenschaftlichen Forschung) grant number 310030_212262.

CONFLICT OF INTEREST STATEMENT

There is no conflict of interest to disclose.

DATA AVAILABILITY STATEMENT

Whole-genome sequence files are available on NCBI, Sequence Read Archive (SRA) (Accession: PRJNA830756). RNA sequencing files are available on NCBI, Gene Expression Omnibus (GEO) (Accession: GSE201323) and SRA (Accession: PRJNA830869).

ORCID

Zeus Jaren Nair https://orcid.org/0000-0001-9662-4958
Kimberly A. Kline https://orcid.org/0000-0002-5472-3074

REFERENCES

Afonina, I., Ong, J., Chua, J., Lu, T. & Kline, K.A. (2020) Multiplex CRISPRi system enables the study of stage-specific biofilm genetic requirements in *Enterococcus faecalis*. *MBio*, 11, e01101–e01120.

Aguilar-Rodríguez, J., Sabater-Muñoz, B., Montagud-Martínez, R., Berlanga, V., Alvarez-Ponce, D., Wagner, A. et al. (2016) The molecular chaperone DnaK is a source of mutational robustness. *Genome Biology and Evolution*, 8, 2979–2991.

Al Mamun, A.A., Lombardo, M.J., Shee, C., Lisewski, A.M., Gonzalez, C., Lin, D. et al. (2012) Identity and function of a large gene network underlying mutagenic repair of DNA breaks. *Science*, 338, 1344–1348.

Anglès, F., Castanié-Cornet, M.-P., Slama, N., Dinclaux, M., Cirinesi, A.-M., Portais, J.-C. et al. (2017) Multilevel interaction of the DnaK/DnaJ(HSP70/HSP40) stress-responsive chaperone machine with the central metabolism. *Scientific Reports*, 7, 41341.

Arends, J., Thomanek, N., Kuhlmann, K., Marcus, K. & Narberhaus, F. (2016) In vivo trapping of FtsH substrates by label-free quantitative proteomics. *Proteomics*, 16, 3161–3172.

Arias, C.A. & Murray, B.E. (2012) The rise of the enterococcus: beyond vancomycin resistance. *Nature Reviews. Microbiology*, 10, 266–278.

Arias, C.A., Panesso, D., Mcgrath, D.M., Qin, X., Mojica, M.F., Miller, C. et al. (2011) Genetic basis for in vivo daptomycin resistance in enterococci. *The New England Journal of Medicine*, 365, 892–900.

Bao, Y., Sakinc, T., Laverde, D., Wobser, D., Benachour, A., Theilacker, C. et al. (2012) Role of mprF1 and mprF2 in the pathogenicity of *Enterococcus faecalis*. *PLoS One*, 7, e38458.

Barák, I. & Muchová, K. (2013) The role of lipid domains in bacterial cell processes. *International Journal of Molecular Sciences*, 14, 4050–4065.

Benjamini, Y. & Hochberg, Y. (1995) Controlling the false discovery rate: a practical and powerful approach to multiple testing. *Journal of the Royal Statistical Society: Series B: Methodological*, 57, 289–300.

Bieniossek, C., Schalch, T., Bumann, M., Meister, M., Meier, R. & Baumann, U. (2006) The molecular architecture of the metalloprotease FtsH. *Proceedings of the National Academy of Sciences of the United States of America*, 103, 3066–3071.

Boshoff, H.I.M., Reed, M.B., Barry, C.E. & Mizrahi, V. (2003) DnaE2 polymerase contributes to in vivo survival and the emergence of drug resistance in mycobacterium tuberculosis. *Cell*, 113, 183–193.

Carmeli, Y., Eliopoulos, G., Mozaffari, E. & Samore, M. (2002) Health and economic outcomes of vancomycin-resistant enterococci. *Archives of Internal Medicine*, 162, 2223–2228.

CH'ng, J.-H., Chong, K.K.L., Lam, L.N., Wong, J.J. & Kline, K.A. (2019) Biofilm-associated infection by enterococci. *Nature Reviews Microbiology*, 17, 82–94.

Dadashi, M., Sharifian, P., Bostanshirin, N., Hajikhani, B., Bostanghadiri, N., Khosravi-Dehaghi, N. et al. (2021) The global prevalence of Daptomycin, Tigecycline, and linezolid-resistant *Enterococcus faecalis* and enterococcus faecium strains from human clinical samples: a systematic review and meta-analysis. *Front Med (Lausanne)*, 8, 720647.

Deuerling, E., Mogk, A., Richter, C., Purucker, M. & Schumann, W. (1997) The ftsH gene of Bacillus subtilis is involved in major cellular processes such as sporulation, stress adaptation and secretion. *Molecular Microbiology*, 23, 921–933.

Do, T., Schaefer, K., Santiago, A.G., Coe, K.A., Fernandes, P.B., Kahne, D. et al. (2020) Staphylococcus aureus cell growth and division are regulated by an amidase that trims peptides from uncrosslinked peptidoglycan. *Nature Microbiology*, 5, 291–303.

Edmond, M.B., Wallace, S.E., Mcclish, D.K., Pfaller, M.A., Jones, R.N. & Wenzel, R.P. (1999) Nosocomial bloodstream infections in United States hospitals: a three-year analysis. *Clinical Infectious Diseases*, 29, 239–244.

Erill, I., Campoy, S. & Barbé, J. (2007) Aeons of distress: an evolutionary perspective on the bacterial SOS response. *FEMS Microbiology Reviews*, 31, 637–656.

Ernst, C.M. & Peschel, A. (2011) Broad-spectrum antimicrobial peptide resistance by MprF-mediated aminoacylation and flipping of phospholipids. *Molecular Microbiology*, 80, 290–299.

Ernst, C.M., Slavetinsky, C.J., Kuhn, S., Hauser, J.N., Nega, M., Mishra, N.N. et al. (2018) Gain-of-function mutations in the phospholipid Flippase MprF confer specific Daptomycin resistance. *MBio*, 9, e01659-18.

Esnaola, M., Puig, P., Gonzalez, D., Castelo, R. & Gonzalez, J.R. (2013) A flexible count data model to fit the wide diversity of expression profiles arising from extensively replicated RNA-seq experiments. *BMC Bioinformatics*, 14, 254.

Fay, A., Philip, J., Saha, P., Hendrickson, R.C., Glickman, M.S. & BURNS-Huang, K. (2021) The DnaK chaperone system buffers the fitness cost of antibiotic resistance mutations in mycobacteria. *MBio*, 12, e00123-21.

García-Fernández, E., Koch, G., Wagner, R.M., Fekete, A., Stengel, S.T., Schneider, J. et al. (2017) Membrane microdomain disassembly inhibits MRSA antibiotic resistance. *Cell*, 171, 1354–1367.e20.

Good, P. (2013) *Permutation tests: a practical guide to resampling methods for testing hypotheses*. New York, NY: Springer.

Harrison, C. (2003) GrpE, a nucleotide exchange factor for DnaK. *Cell Stress & Chaperones*, 8, 218–224.

Hayer-Hartl, M., Bracher, A. & Hartl, F.U. (2016) The GroEL–GroES chaperonin machine: a Nano-cage for protein folding. *Trends in Biochemical Sciences*, 41, 62–76.

Hidron, A.I., Edwards, J.R., Patel, J., Horan, T.C., Sievert, D.M., Pollock, D.A. et al. (2008) NHSN annual update: antimicrobial-resistant pathogens associated with healthcare-associated infections: annual summary of data reported to the National Healthcare Safety Network at the Centers for Disease Control and Prevention, 2006-2007. *Infection Control and Hospital Epidemiology*, 29, 996–1011.

Hollenbeck, B.L. & Rice, L.B. (2012) Intrinsic and acquired resistance mechanisms in enterococcus. *Virulence*, 3, 421–569.

Kamal, S.M., Rybtke, M.L., Nimtz, M., Sperlein, S., Giske, C., Trček, J. et al. (2019) Two FtsH proteases contribute to fitness and adaptation of *Pseudomonas aeruginosa* clone C strains. *Frontiers in Microbiology*, 10, 1372.

Kelesidis, T., Humphries, R., Uslan, D.Z. & Pegues, D.A. (2011) Daptomycin nonsusceptible enterococci: an emerging challenge for clinicians. *Clinical Infectious Diseases*, 52, 228–234.

Khan, A., Davlieva, M., Panesso, D., Rincon, S., Miller, W.R., Diaz, L. et al. (2019) Antimicrobial sensing coupled with cell membrane remodeling mediates antibiotic resistance and virulence in *enterococcus faecalis*. *Proceedings of the National Academy of Sciences*, 116, 26925–26932.

Kristich, C.J., Nguyen, V.T., Le, T., Barnes, A.M., Grindle, S. & Dunny, G.M. (2008) Development and use of an efficient system for random mariner transposon mutagenesis to identify novel genetic determinants of biofilm formation in the core *Enterococcus faecalis* genome. *Applied and Environmental Microbiology*, 74, 3377–3386.

Langklotz, S., Baumann, U. & Narberhaus, F. (2012) Structure and function of the bacterial AAA protease FtsH. *Biochimica et Biophysica Acta (BBA) - Molecular Cell Research*, 1823, 40–48.

Li, L., Higgs, C., Turner, A.M., Nong, Y., Gorrie, C.L., Sherry, N.L. et al. (2021) Daptomycin resistance occurs predominantly in vanA-type vancomycin-resistant enterococcus faecium in Australasia and is associated with heterogeneous and novel mutations. *Frontiers in Microbiology*, 12, 749935.

Li, W., Hu, J., Li, L., Zhang, M., Cui, Q., Ma, Y. et al. (2022) New mutations in cls Lead to Daptomycin resistance in a clinical vancomycin- and Daptomycin-resistant enterococcus faecium strain. *Frontiers in Microbiology*, 13, 896916.

Liu, W., Schoonen, M., Wang, T., Mcsweeney, S. & Liu, Q. (2022) Cryo-EM structure of transmembrane AAA+ protease FtsH in the ADP state. *Communications Biology*, 5, 257.

Lopez, D. & Koch, G. (2017) Exploring functional membrane microdomains in bacteria: an overview. *Current Opinion in Microbiology*, 36, 76–84.

Maddalo, G., Chovanec, P., STENBERG-Bruzell, F., Nielsen, H.V., Jensen-Seaman, M.I., Ilag, L.L. et al. (2011) A reference map of the membrane proteome of *Enterococcus faecalis*. *Proteomics*, 11, 3935–3941.

Mascini, E.M. & Bonten, M.J.M. (2005) Vancomycin-resistant enterococci: consequences for therapy and infection control. *Clinical Microbiology and Infection*, 11, 43–56.

Merrikh, H. & Kohli, R.M. (2020) Targeting evolution to inhibit antibiotic resistance. *The FEBS Journal*, 287, 4341–4353.

Miller, C., Kong, J., Tran, T.T., Arias, C.A., Saxer, G. & Shamoo, Y. (2013) Adaptation of *Enterococcus faecalis* to daptomycin reveals an ordered progression to resistance. *Antimicrobial Agents and Chemotherapy*, 57, 5373–5383.

Miller, W.R., Bayer, A.S. & Arias, C.A. (2016) Mechanism of action and resistance to Daptomycin in Staphylococcus aureus and enterococci. *Cold Spring Harbor Perspectives in Medicine*, 6, a026997.

Miller, W.R., Munita, J.M. & Arias, C.A. (2014) Mechanisms of antibiotic resistance in enterococci. *Expert Review of Anti-Infective Therapy*, 12, 1221–1236.

Miller, W.R., Murray, B.E., Rice, L.B. & Arias, C.A. (2020) Resistance in Vancomycin-Resistant Enterococci. *Infectious Disease Clinics of North America*, 34, 751–771.

Mishra, N.N., Bayer, A.S., Tran, T.T., Shamoo, Y., Mileykovskaya, E., Dowhan, W. et al. (2012) Daptomycin resistance in enterococci is associated with distinct alterations of cell membrane phospholipid content. *PLoS One*, 7, e43958.

Mishra, N.N., Lew, C., Abdelhady, W., Lapitan, C.K., Proctor, R.A., Rose, W.E. et al. (2022) Synergy mechanisms of Daptomycin-Fosfomycin combinations in Daptomycin-susceptible and -resistant methicillin-resistant Staphylococcus aureus: in vitro, ex vivo, and in vivo metrics. *Antimicrobial Agents and Chemotherapy*, 66, e0164921.

Mishra, N.N., Yang, S.-J., Sawa, A., Rubio, A., Nast, C.C., Yeaman, M.R. et al. (2009) Analysis of cell membrane characteristics of in vitro-selected daptomycin-resistant strains of methicillin-resistant Staphylococcus aureus. *Antimicrobial Agents and Chemotherapy*, 53, 2312–2318.

Müller, A., Wenzel, M., Strahl, H., Grein, F., Saaki, T.N.V., Kohl, B. et al. (2016) Daptomycin inhibits cell envelope synthesis by interfering with fluid membrane microdomains. *Proceedings of the National Academy of Sciences*, 113, E7077–E7086.

Munita, J.M., Murray, B.E. & Arias, C.A. (2014) Daptomycin for the treatment of bacteraemia due to vancomycin-resistant enterococci. *International Journal of Antimicrobial Agents*, 44, 387–395.

Munoz-Price, L.S., Lolans, K. & Quinn, J.P. (2005) Emergence of resistance to Daptomycin during treatment of vancomycin-resistant *Enterococcus faecalis* infection. *Clinical Infectious Diseases*, 41, 565–566.

Murdoch, D.R., Corey, G.R., Hoen, B., Miro, J.M., Fowler, V.G., Jr., Bayer, A.S. et al. (2009) Clinical presentation, etiology, and outcome of infective endocarditis in the 21st century: the international collaboration on endocarditis-prospective cohort study. *Archives of Internal Medicine*, 169, 463–473.

Niwa, H., Tsuchiya, D., Makyio, H., Yoshida, M. & Morikawa, K. (2002) Hexameric ring structure of the ATPase domain of the membrane-integrated metalloprotease FtsH from Thermus thermophilus HB8. *Structure*, 10, 1415–1424.

Okuno, T. & Ogura, T. (2013) FtsH protease-mediated regulation of various cellular functions. *Sub-Cellular Biochemistry*, 66, 53–69.

Ota, Y., Furuhashi, K., Hayashi, W., Hirai, N., Ishikawa, J., Nagura, O. et al. (2021) Daptomycin resistant *Enterococcus faecalis* has a mutation in liaX, which encodes a surface protein that inhibits the LiaFSR systems and cell membrane remodeling. *Journal of Infection and Chemotherapy*, 27, 90–93.

Palmer, K.L., Daniel, A., Hardy, C., Silverman, J. & Gilmore, M.S. (2011) Genetic basis for daptomycin resistance in enterococci. *Antimicrobial Agents and Chemotherapy*, 55, 3345–3356.

Patel, R. & Gallagher, J.C. (2015) Vancomycin-resistant enterococcal bacteremia pharmacotherapy. *The Annals of Pharmacotherapy*, 49, 69–85.

Patterson, J.E., Sweeney, A.H., Simms, M., Carley, N., Mangi, R., Sabetta, J. et al. (1995) An analysis of 110 serious enterococcal infections. Epidemiology, antibiotic susceptibility, and outcome. *Medicine (Baltimore)*, 74, 191–200.

Pfaller, M.A., Cormican, M., Flamm, R.K., Mendes, R.E. & Jones, R.N. (2019) Temporal and geographic variation in antimicrobial susceptibility and resistance patterns of enterococci: results from the SENTRY antimicrobial surveillance program, 1997-2016. *Open Forum Infectious Diseases*, 6, S54–S62.

Prater, A.G., Mehta, H.H., Beabout, K., Supandy, A., Miller, W.R., Tran, T.T. et al. (2021) Daptomycin resistance in enterococcus faecium can Be delayed by disruption of the LiaFSR stress response pathway. *Antimicrobial Agents and Chemotherapy*, 65, e01317–e01320.

Prematunge, C., Macdougall, C., Johnstone, J., Adomako, K., Lam, F., Robertson, J. et al. (2016) VRE and VSE bacteremia outcomes in the era of effective VRE therapy: a systematic review and meta-analysis. *Infection Control and Hospital Epidemiology*, 37, 26–35.

Ragheb, M.N., Thomason, M.K., Hsu, C., Nugent, P., Gage, J., Samadpour, A.N. et al. (2019) Inhibiting the evolution of antibiotic resistance. *Molecular Cell*, 73, 157–165.e5.

Rashid, R., Cazenave-Gassiot, A., Gao, I.H., Nair, Z.J., Kumar, J.K., Gao, L. et al. (2017) Comprehensive analysis of phospholipids and glycolipids in the opportunistic pathogen *Enterococcus faecalis*. *PLoS One*, 12, e0175886.

Rashid, R., Nair, Z.J., Chia, D.M.H., Chong, K.K.L., Gassiot, A.C., Morley, S.A. et al. (2023) Depleting cationic lipids involved in antimicrobial resistance drives adaptive lipid remodeling in *Enterococcus faecalis*. *MBio*, 14, e03073-22.

Rashid, R., Veleba, M. & Kline, K.A. (2016) Focal targeting of the bacterial envelope by antimicrobial peptides. *Frontiers in Cell and Developmental Biology*, 4, 55.

Reinseth, I.S., Ovchinnikov, K.V., Tønnesen, H.H., Carlsen, H. & Diep, D.B. (2020) The increasing issue of vancomycin-resistant enterococci and the Bacteriocin solution. *Probiotics and Antimicrobial Proteins*, 12, 1203–1217.

Reyes, J., Panesso, D., Tran, T.T., Mishra, N.N., Cruz, M.R., Munita, J.M. et al. (2015) A liaR deletion restores susceptibility to daptomycin and antimicrobial peptides in multidrug-resistant *Enterococcus faecalis*. *The Journal of Infectious Diseases*, 211, 1317–1325.

Sabat, A.J., Tinelli, M., Grundmann, H., Akkerboom, V., Monaco, M., del Grosso, M. et al. (2018) Daptomycin resistant Staphylococcus aureus clinical strain with novel non-synonymous mutations in the mprF and vraS genes: a new insight into Daptomycin resistance. *Frontiers in Microbiology*, 9, 2705.

Satlin, M.J., Nicolau, D.P., Humphries, R.M., Kuti, J.L., Campeau, S.A., Lewis Ii, J.S. et al. (2019) Development of Daptomycin susceptibility breakpoints for enterococcus faecium and revision of the breakpoints for other Enterococcal species by the clinical and laboratory standards institute. *Clinical Infectious Diseases*, 70, 1240–1246.

Schumann, W. (2016) Regulation of bacterial heat shock stimulons. *Cell Stress & Chaperones*, 21, 959–968.

Shoemaker, D.M., Simou, J. & Roland, W.E. (2006) A review of daptomycin for injection (Cubicin) in the treatment of complicated skin and skin structure infections. *Therapeutics and Clinical Risk Management*, 2, 169–174.

Sinel, C., Cosquer, T., Auzou, M., Goux, D., Giard, J.-C. & Cattoir, V. (2016) Sequential steps of daptomycin resistance in enterococcus faecium and reversion to hypersusceptibility through IS-mediated inactivation of the liaFSR operon. *Journal of Antimicrobial Chemotherapy*, 71, 2793–2797.

Song, X., Srinivasan, A., Plaut, D. & Perl, T.M. (2003) Effect of nosocomial vancomycin-resistant enterococcal bacteremia on mortality, length of stay, and costs. *Infection Control and Hospital Epidemiology*, 24, 251–256.

Steenbergen, J.N., Alder, J., Thorne, G.M. & Tally, F.P. (2005) Daptomycin: a lipopeptide antibiotic for the treatment of serious gram-positive infections. *The Journal of Antimicrobial Chemotherapy*, 55, 283–288.

Stinemetz, E.K., Gao, P., Pinkston, K.L., Montealegre, M.C., Murray, B.E. & Harvey, B.R. (2017) Processing of the major autolysin of *E. Faecalis*, AtlA, by the zinc-metalloprotease, GelE, impacts AtlA septal localization and cell separation. *PLoS One*, 12, e0186706.

Sulaiman, J.E. & Lam, H. (2021) Novel Daptomycin tolerance and resistance mutations in methicillin-resistant Staphylococcus aureus from adaptive laboratory evolution. *mSphere*, 6, e0069221.

Suomi, T., Seyednasrollah, F., Jaakkola, M.K., Faux, T. & Elo, L.L. (2017) ROTS: an R package for reproducibility-optimized statistical testing. *PLoS Computational Biology*, 13, e1005562.

Taylor, S.D. & Palmer, M. (2016) The action mechanism of daptomycin. *Bioorganic & Medicinal Chemistry*, 24, 6253–6268.

Tran, T.T., Munita, J.M. & Arias, C.A. (2015) Mechanisms of drug resistance: daptomycin resistance. *Annals of the New York Academy of Sciences*, 1354, 32–53.

Tran, T.T., Panesso, D., Gao, H., Roh, J.H., Munita, J.M., Reyes, J. et al. (2013) Whole-genome analysis of a Daptomycin-susceptible enterococcus faecium strain and its Daptomycin-resistant variant arising during therapy. *Antimicrobial Agents and Chemotherapy*, 57, 261–268.

Tran, T.T., Panesso, D., Mishra, N.N., Mileykovskaya, E., Guan, Z., Munita, J.M. et al. (2013) Daptomycin-resistant *Enterococcus faecalis* diverts the antibiotic molecule from the division septum and remodels cell membrane phospholipids. *MBio*, 4, e00281-13.

Vollmer, W., Joris, B., Charlier, P. & Foster, S. (2008) Bacterial peptidoglycan (murein) hydrolases. *FEMS Microbiology Reviews*, 32, 259–286.

Wang, G., Yu, F., Lin, H., Murugesan, K., Huang, W., Hoss, A.G. et al. (2018) Evolution and mutations predisposing to daptomycin resistance in vancomycin-resistant enterococcus faecium ST736 strains. *PLoS One*, 13, e0209785.

Weiner, L.M., Webb, A.K., Limbago, B., Dudeck, M.A., Patel, J., Kallen, A.J. et al. (2016) Antimicrobial-resistant pathogens associated with healthcare-associated infections: summary of data reported to the National Healthcare Safety Network at the Centers for Disease Control and Prevention, 2011-2014. *Infection Control and Hospital Epidemiology*, 37, 1288–1301.

Wiegand, I., Hilpert, K. & Hancock, R.E. (2008) Agar and broth dilution methods to determine the minimal inhibitory concentration (MIC) of antimicrobial substances. *Nature Protocols*, 3, 163–175.

Yepes, A., Schneider, J., Mielich, B., Koch, G., García-Betancur, J.C., Ramamurthi, K.S. et al. (2012) The biofilm formation defect of a Bacillus subtilis flotillin-defective mutant involves the protease FtsH. *Molecular Microbiology*, 86, 457–471.

Zarb, P., Coignard, B., Griskeviciene, J., Muller, A., Vankerckhoven, V., Weist, K. et al. (2012) The European Centre for Disease Prevention and Control (ECDC) pilot point prevalence survey of healthcare-associated infections and antimicrobial use. *Eurosurveillance*, 17, 20316.

SUPPORTING INFORMATION

Additional supporting information can be found online in the Supporting Information section at the end of this article.

How to cite this article: Nair, Z.J., Gao, I.H., Firras, A., Chong, K.K.L., Hill, E.D., Choo, P.Y. et al. (2024) An essential protease, FtsH, influences daptomycin resistance acquisition in *Enterococcus faecalis*. *Molecular Microbiology*, 121, 1021–1038. Available from: https://doi.org/10.1111/mmi.15253